Nitric Oxide Synthase Inhibitors That Interact with Both Heme Propionate and Tetrahydrobiopterin Show High Isoform Selectivity

Soosung Kang,[†] Wei Tang,[†] Huiying Li,[‡] Georges Chreifi,[‡] Pavel Martásek,[§] Linda J. Roman,[§] Thomas L. Poulos,*[‡] and Richard B. Silverman*[†]

[†]Department of Chemistry, Department of Molecular Biosciences, Chemistry of Life Processes Institute, Center for Molecular Innovation and Drug Discovery, Northwestern University, Evanston, Illinois 60208-3113, United States

[‡]Departments of Molecular Biology and Biochemistry, Pharmaceutical Sciences, and Chemistry, University of California, Irvine, California 92697-3900, United States

[§]Department of Biochemistry, University of Texas Health Science Center, San Antonio, Texas 78384-7760, United States

Ⓢ *Supporting Information*
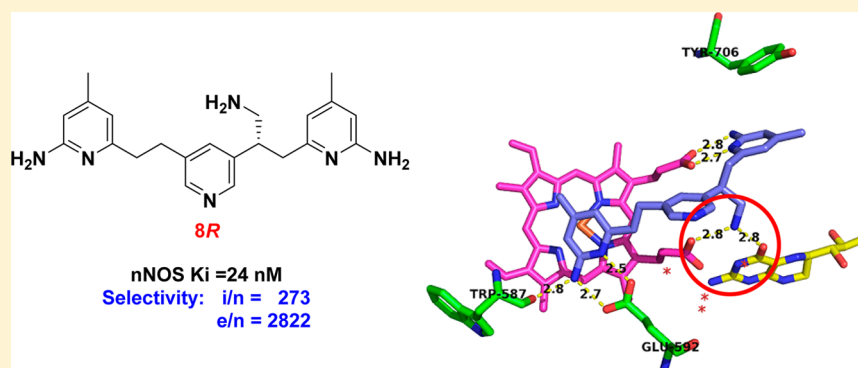
ABSTRACT: Overproduction of NO by nNOS is implicated in the pathogenesis of diverse neuronal disorders. Since NO signaling is involved in diverse physiological functions, selective inhibition of nNOS over other isoforms is essential to minimize side effects. A series of α-amino functionalized aminopyridine derivatives (**3–8**) were designed to probe the structure−activity relationship between ligand, heme propionate, and H_4B. Compound **8R** was identified as the most potent and selective molecule of this study, exhibiting a K_i of 24 nM for nNOS, with 273-fold and 2822-fold selectivity against iNOS and eNOS, respectively. Although crystal structures of **8R** complexed with nNOS and eNOS revealed a similar binding mode, the selectivity stems from the distinct electrostatic environments in two isoforms that result in much lower inhibitor binding free energy in nNOS than in eNOS. These findings provide a basis for further development of simple, but even more selective and potent, nNOS inhibitors.

■ INTRODUCTION

The free radical nitric oxide (NO) is an important signaling molecule,[1] controlling diverse physiological and pathological processes in various species.[2] In mammals, NO is endogenously produced using L-arginine and molecular oxygen with NADPH by three principal nitric oxide synthases (NOSs): neuronal NOS (nNOS), endothelial NOS (eNOS), and inducible NOS (iNOS).[3] Selective inhibition of each NOS can regulate different biological functions of NO signaling because each NOS isoform is localized differently in the neuron, endothelium, and immune system, and is activated by a specific pathway.[4] Overproduction of NO by nNOS in the central nervous system has been implicated in the pathogenesis of diverse neuronal disorders such as strokes,[5] septic shock,[6] seizures,[7] migraine headaches,[8] Alzheimer's disease,[9] Parkinson's disease,[10] and ALS.[11] Recently, nNOS has also been implicated to play a critical role in melanoma tumor development and growth.[12] In the immune system, excess NO production from iNOS is also linked to inflammation and

various cancers.[13] In addition, NO synthesis from bacterial NOS was reported to play a critical role in antibiotic resistance and pathogenicity.[14,15] This suggests that the inhibition of NOSs can be effective for the control of these diverse diseases, but because NO signaling is involved in various physiological functions, selective inhibition is essential to minimize any unwanted side effects.[16]

NOSs are homodimeric enzymes; each monomer consists of a reductase domain and an oxygenase domain. A C-terminal reductase domain contains NADPH, FAD, and FMN cofactors,[17] and an N-terminal oxygenase domain contains iron protoporphyrin IX (heme), where the substrate L-Arg binds, and tetrahydrobiopterin (H_4B) cofactors.[18] H_4B forms tight H-bonds with the propionate of the heme A-ring and provides an electron that is crucial for activating the heme-bound dioxygen during the catalytic reaction.[19] Although H_4B
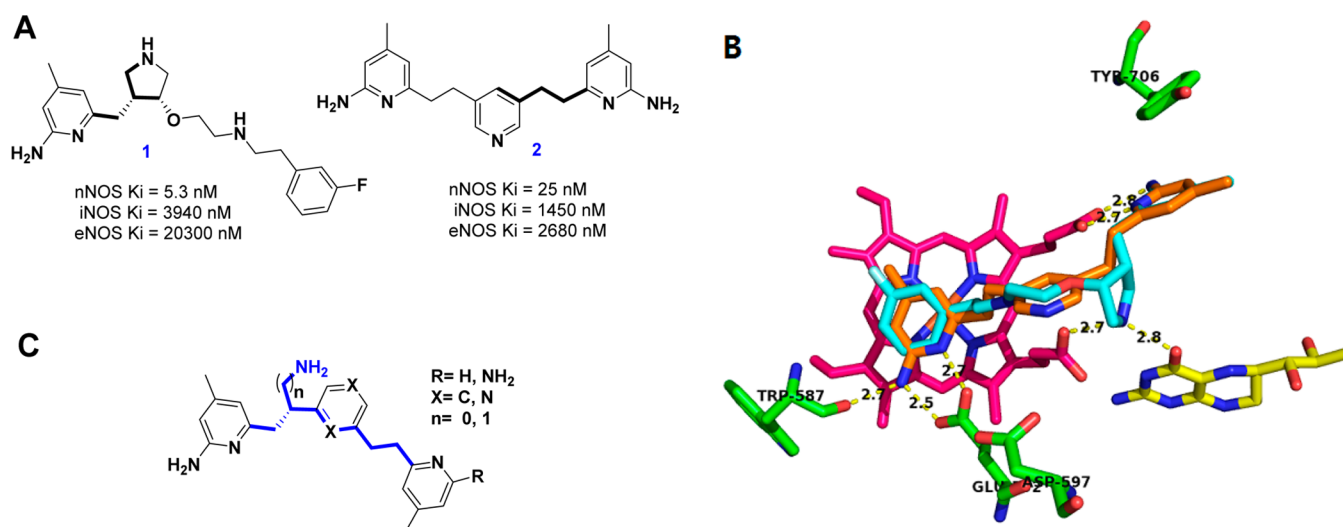
Figure 1. (a) Chemical structures of leads **1** and **2** and inhibitory activities; (b) overlay of inhibitors **1** (cyan) and **2** (orange) complexed with nNOS, showing the heme (pink), H_4B (yellow), and key residues (green) in the active site (PDB: 3NLM and 3N5W); and (c) the proposed scaffold derived from compounds **1** and **2**.
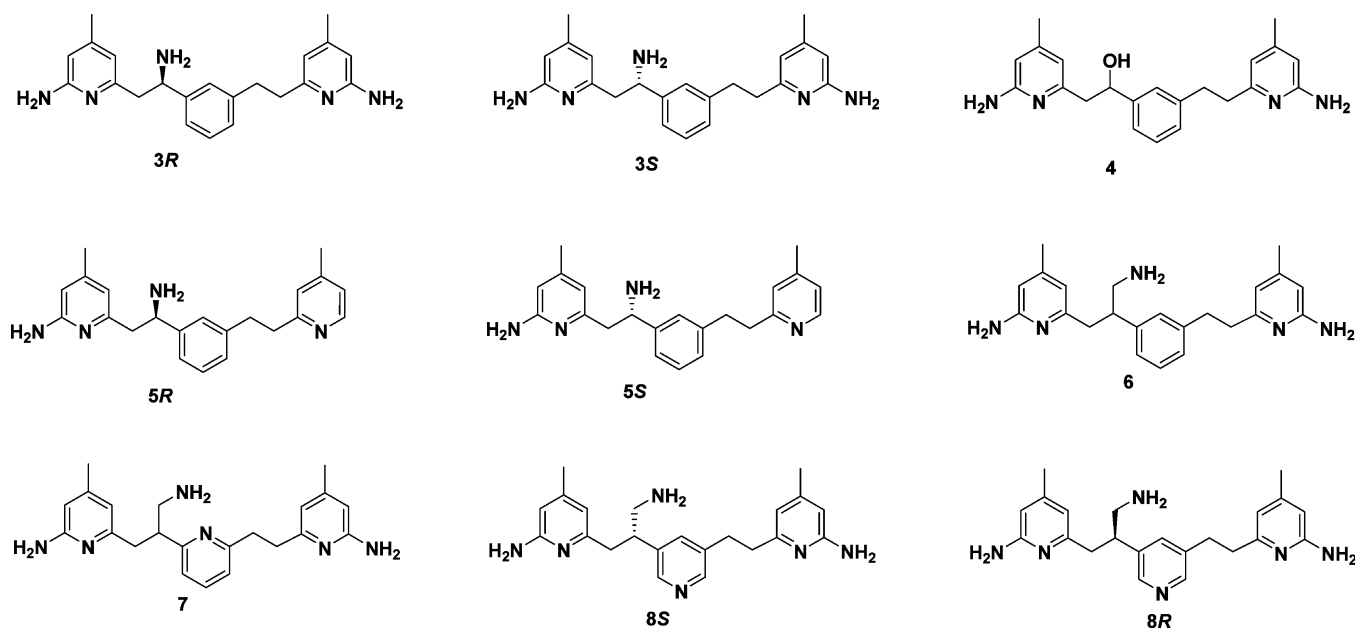

**Figure 2.** Prepared and tested molecules in this study.

binding is not required for dimerization, it interacts with both subunits of the dimer by forming part of the dimerization interface to enrich the structural stability of the dimer.[20,21]

For over a decade, our research groups have been interested in the development of selective inhibitors of nNOS for the treatment of neurodegenerative disease. Among diverse NOS inhibitors, compounds **1**[22] and **2**[23] (Figure 1A) are the most potent inhibitors for nNOS. They are spotlighted by excellent isoform selectivity for **1** and easy synthesis for **2**. Compound **1** has >700-fold selectivity against iNOS and >3800-fold selectivity against eNOS. The X-ray crystal structures of **1** complexed with nNOS and eNOS[24] reveal features of enzyme–inhibitor interactions that form the basis for high potency and selectivity (Figure 1B): the aminopyridine of **1** interacts with a heme D-ring propionate via two H-bonds, as well as with Tyr706 in a π−π stacking interaction. The pyrrolidine nitrogen of **1** is located within hydrogen-bonding distances to both H_4B

and the heme A-ring propionate, replacing a water molecule, while the fluorophenyl ring stacks with the heme plane. Despite the excellent isoform selectivity of this molecule, the construction of the two unnaturally occurring chiral centers of **1** is not efficient and requires multiple steps with a low overall yield. This limits the opportunities for optimizing the pharmacokinetic properties of the inhibitor and for carrying out in vivo studies. Compound **2**, the other potent nNOS inhibitor (K_i = 25 nM), is only moderately selective (i/n = 58, e/n = 107) but can be prepared from commercial starting materials in four chemical steps, in an excellent overall yield. The common feature of **1** and **2** is that both utilize one aminopyridine to make H-bonds with the heme D-ring propionate and to stack with Tyr706 (Figure 1B). The additional H-bonds between the other aminopyridine of **2** and Glu592 of nNOS anchor the inhibitor to the substrate binding site above the heme in a double-headed mode. However, **2**, in contrast to **1**, does not

Scheme 1. Synthesis of 3R and 3S[a]
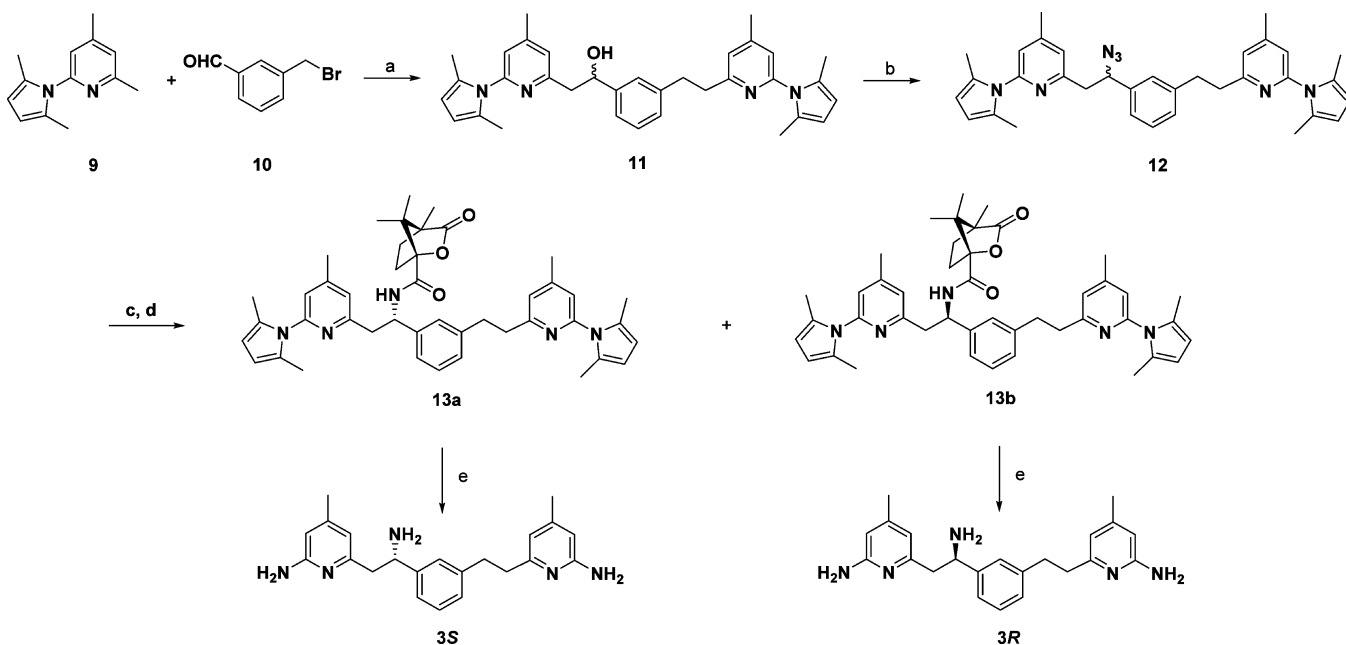
[a]Reagents and conditions: (a) **9** (2.5 equiv), BuLi (2.5 equiv), THF, 0 °C to −78 °C; (b) DEAD, DPPA, PPh$_3$, THF, room temp., 12 h; (c) LiAlH$_4$; (d) (i) (S)-camphamic chloride, TEA, CH$_2$Cl$_2$, room temp., (ii) chiral resolution on a silica gel column; (e) conc HCl, AcOH, microwave, 150 °C, 5 h.

Scheme 2. Synthesis of 5R and 5S[a]
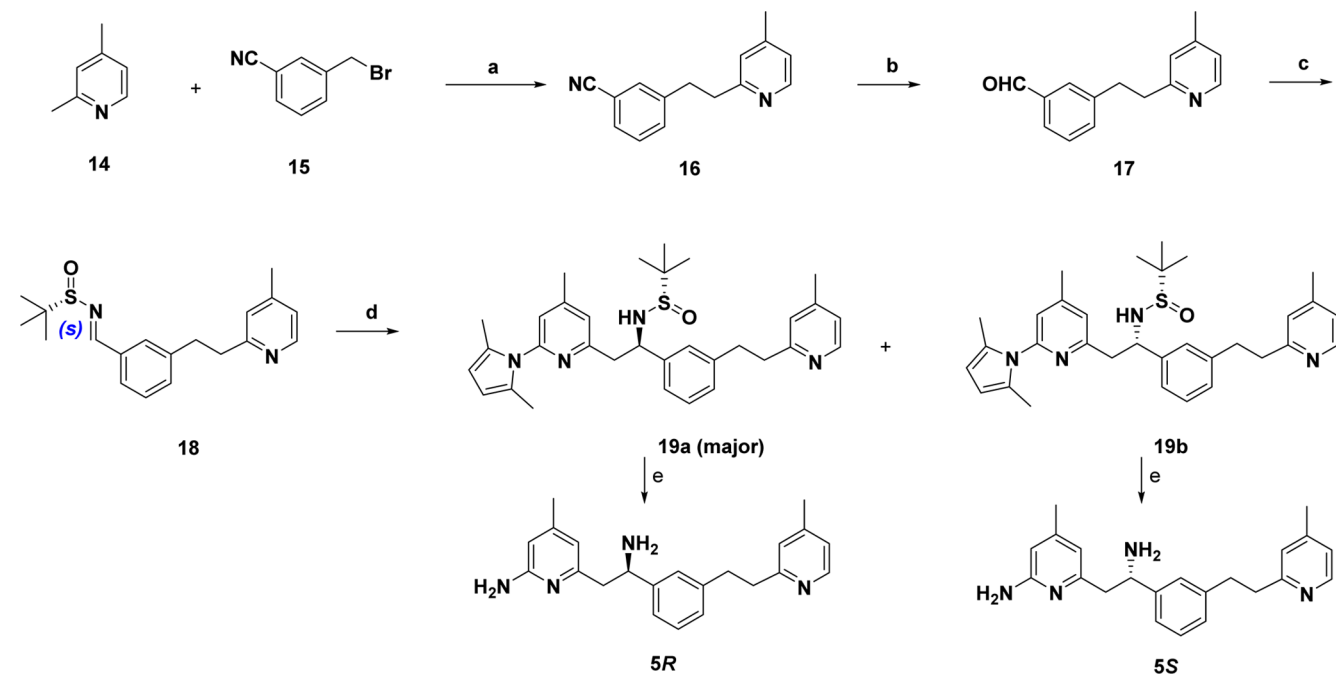
[a]Reagents and conditions; (a) BuLi, THF; (b) DIBAL; (c) (S)-t-butylsulfinamide, Ti(OEt)$_4$; (d) **9**, BuLi; (e) conc HCl, EtOH, microwave, 120 °C, 20 min.

directly interact with the H$_4$B or with the propionate of the heme A-ring. The lack of these interactions may explain the moderate selectivity of **2** against iNOS and eNOS.

A possible strategy to confirm this structure-selectivity issue is to install a new functional group on molecule **2** to create an interaction with H$_4$B and the heme A-ring propionate. This approach will allow us to perform a SAR study in this area for a

new chemotype design in which the molecules will be easy to prepare while still being highly isoform selective. From the structure overlay of **1** and **2** (Figure 1B), we found that the pyrrolidine amine of **1** could be replaced by the addition of an amino group on the side chain of **2** (Figure 1C). The alignment of an amino group with an adapting position of the middle aromatic ring of **2**, especially maintaining the structural

Scheme 3. Synthesis of 5[a]
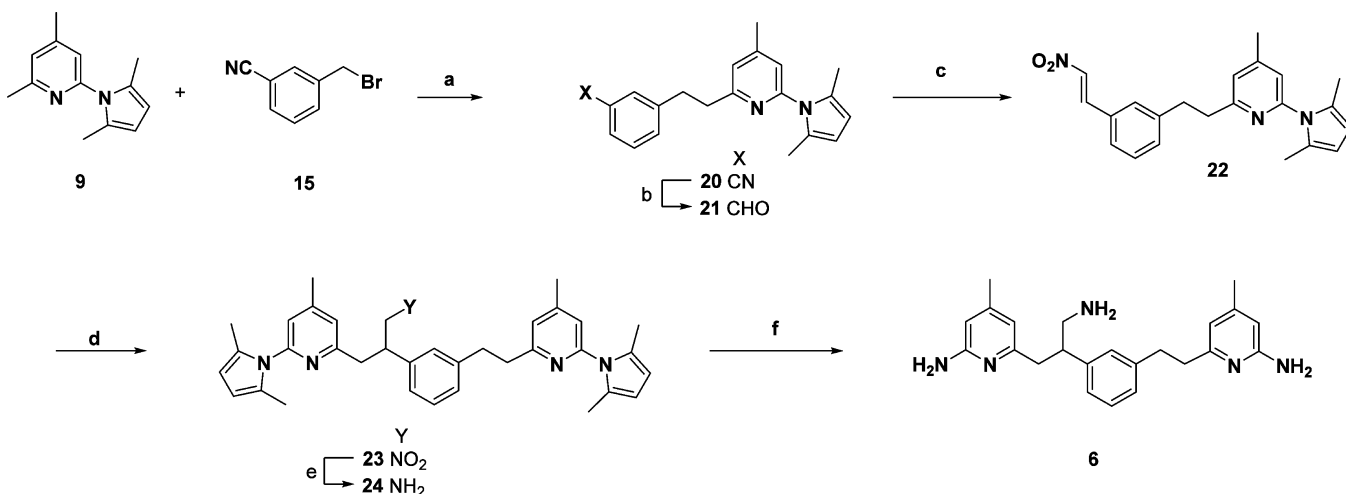
[a]Reagents and conditions: (a) (i) **9**, BuLi, THF; (ii) **15**; (b) DIBAL-H; (c) (i) MeNO$_2$, TEA, (ii) AcCl; (d) **9**, BuLi; (e) LAH; (f) conc HCl, EtOH, microwave, 120 °C, 20 min.

Scheme 4. Synthesis of 7 and 8[a]
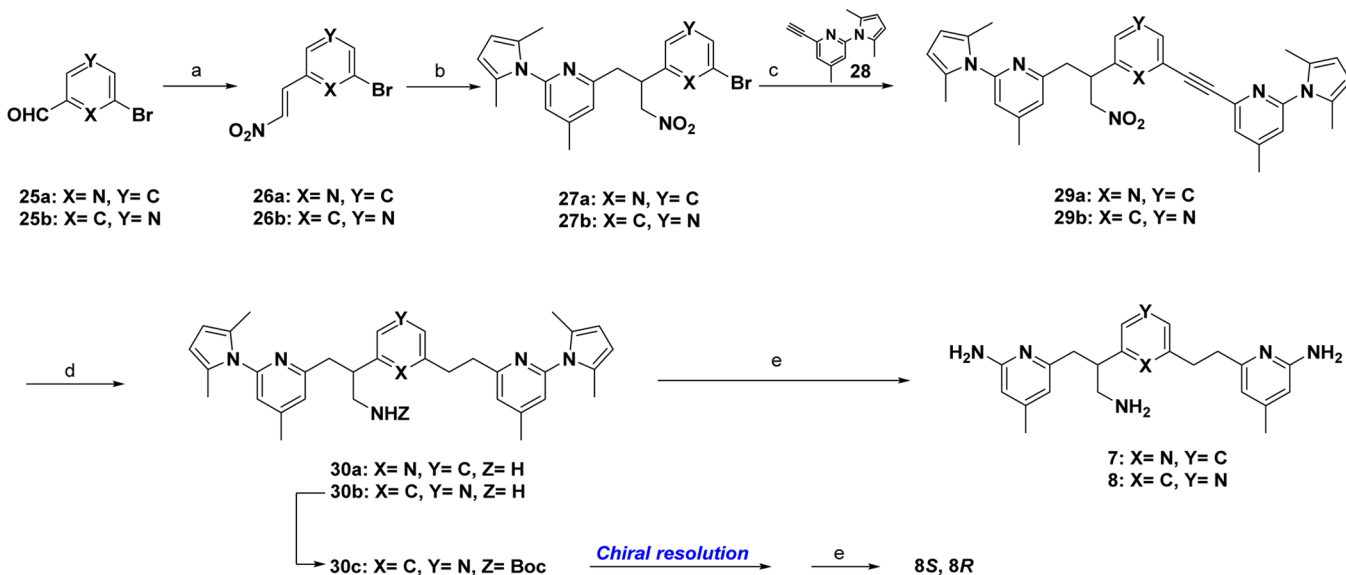
[a]Reagents and conditions: (a) (i) MeNO$_2$, TEA, (ii) AcCl; (b) **9**, BuLi; (c) **28**, Pd(PPh$_3$)$_2$Cl$_2$, CuI, PPh$_3$, DEA, DMF; (d) Raney-Ni, H$_2$, MeOH/EtOH; (e) conc HCl/EtOH (1/2), microwave, 120 °C, 20 min.

similarity to the pyrrolidine amine of **1**, was virtually performed using Surflex-Sim in the Sybyl-X program. Although the *R*-enantiomer of the α-amino derivative was predicted to interact with H$_4$B and a propionate of the heme, the preparation of the other enantiomer was also desirable to confirm the stereo-activity relationship. After 2-amino-4-methylpyridine was selected as a head near the α-amino group, three different meta-substituted aromatic rings were adapted as linkers, and another 2-amino-4-methylpyridine or a 4-methylpyridine ring was chosen as the second head in the hopes that it would stay above the heme with a proposed interaction with Glu592. The crystal structural information gathered with compounds bearing an α-amino group (**3−5**) led to the introduction of an aminomethyl group (**6−8**) to further improve the binding affinity and selectivity. Figure 2 summarizes the prepared and assayed compounds in this study.

■ CHEMISTRY

The synthesis of compounds **3R** and **3S** is shown in Scheme 1. Benzyl alcohol **11** was prepared by coupling of 3-bromomethylbenzaldehyde (**9**) with two equivalents of lithiated pyrrolyl-4,6-lutidine (**10**). The hydroxyl group of **11** was then converted to benzyl azide **12** via a Mitsunobu reaction with DPPA. Reduction of the azide with LiAlH$_4$ gave the free amine, which subsequently underwent amidation with (*S*)-camphanic chloride to give a separable diastereomeric mixture. Each pure diastereomer, **13a** and **13b**, was successfully isolated using general silica gel column chromatography. An asymmetric approach toward the target compounds using Ellman's chiral sulfinamide in the synthesis of **4R** and **4S** (Scheme 2) was not successful; only inseparable diastereomeric mixtures were produced. The (*S*)-camphanyl auxiliary and the two protecting groups on the aminopyridine rings were removed together by

Table 1. List of K_i Values and Selectivity of 3–8

Name	structure	nNOS Ki (nM)	iNOS Ki (nM)	eNOS Ki (nM)	i/n	e/n
3S		144 (±11)	17,670 (±1,982)	70,900 (±2,163)	123	492
3R		122 (±9)	15,620 (±1,210)	14,390 (±1,053)	128	118
4		70 (±4)	5,990 (±563)	3,610 (±320)	86	52
5S		903 (±81)	>100,000	328,000 (±25,000)	>110	363
5R		4,370 (±68)	>100,000	1049,000 (±31,000)	>22	240
6		53 (±5)	1,894 (±138)	4,770 (±55)	36	90
7		123 (±7)	17,916 (±1,296)	133,174 (±10,330)	138	1072
8		30 (±4)	2,810 (±192)	16,000 (±1,438)	95	544
2[a]		25	1,450	2,680	58	107
31[a]		49	682	1,410	14	29
32[a]		99	4,750	9,400	48	95

[a]Reference molecules that were reported previously.[23]

microwave-aided hydrolysis to give optically active **3R** and **3S** (Scheme 1).

Compounds **5R** and **5S** were prepared from 2,4-dimethyllutidine and **15** using a five-step procedure (Scheme 2). Lithiated 2,4-dimethyllutidine was coupled with benzyl bromide **15** to give nitrile **16**. The cyano group of **16** was reduced to an aldehyde (**17**) using DIBAL, which then underwent condensation with Ellman's chiral sulfinamide to give (S)-N-tert-butanesulfinyl aldimine **18** in a moderate yield. This intermediate was coupled with lithiated pyrrolyl-4,6-lutidine **9** to give diastereomeric mixture **19a–b**. Minor diastereomeric product **19b** eluted first, and the major product **19a** eluted second during silica gel column chromatography. Protecting groups on the aminopyridine and t-butyl sulfinamide of **19a**

and **19b** were removed by microwave-aided acidic hydrolysis to give **5R** and **5S** in high yields.

Compound **6** was also prepared from benzyl bromide **15** using a six-step procedure (Scheme 3). Coupling of lithiated **9** with **15** gave nitrile **20**, which was then reduced to aldehyde **21** by treatment with DIBAL. Condensation of **21** with nitromethane gave nitrovinyl compound **22** in good yield. Michael addition of **22** with lithiated **9** produced nitro intermediate **23**, which was reduced to amine **24** using Raney-Ni under a hydrogen atmosphere. Both aminopyridine protecting groups were removed by microwave-aided hydrolysis to give **6** in good yields.

Compounds **7** and **8** were prepared in five steps from commercially available brominated pyridinylaldehydes **25a–b**

Table 2. K_i Values and Selectivity of 8S and 8R

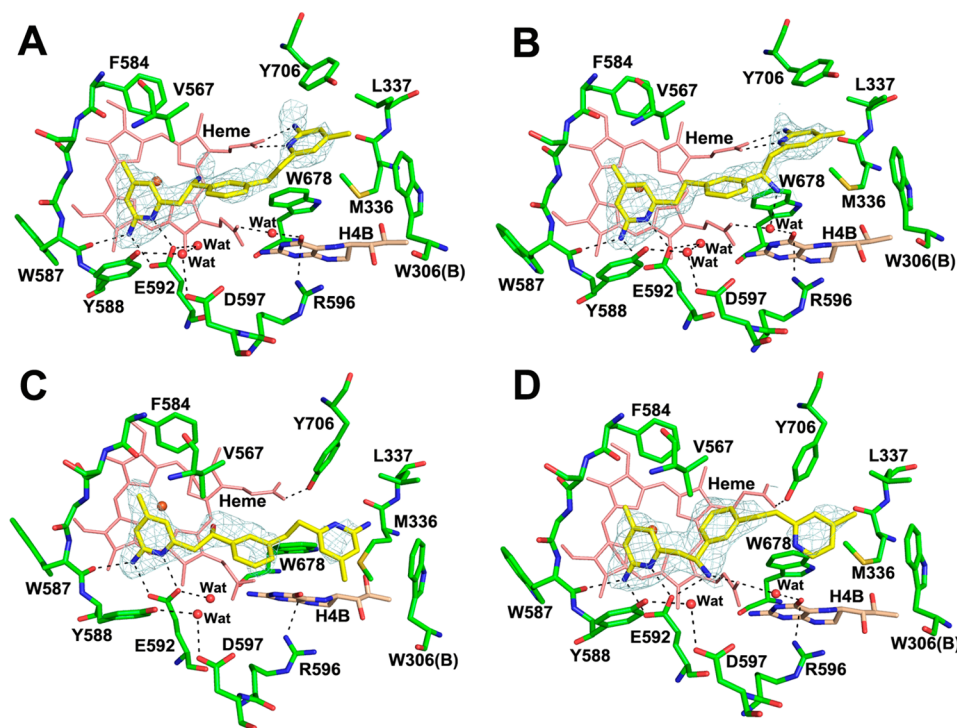| Name	structure	nNOS Ki (nM)	iNOS Ki (nM)	eNOS Ki (nM)	i/n	e/n
8S		70 (±4)	4,386 (±394)	19,417 (±1,058)	105	276
8R		24 (±2)	6,629 (±561)	68,520 (±4,817)	273	2,822

Figure 3. Active site structures of rat nNOS in complex with (A) **3S** (PDB: 4CTP), (B) **3R** (PDB: 4CTQ), (C) **4** (PDB: 4CTR), and (D) **5** or **5S** (PDB: 4CTT). The $F_o − F_c$ omit electron density for the inhibitor is displayed at the 2.5 σ contour level. The weaker density in the tail part of **4** and **5** indicates disordering. The major H-bonds are depicted with dashed lines. All crystal structure figures were prepared with PyMol (www.pymol.org).

(Scheme 4). Condensation of **25a−b** with nitromethane in the presence of TEA and acetyl chloride, followed by Michael reaction with lithiated 4,6-dimethylpyridine afforded **27a−b**. Sonogashira coupling between **27a−b** and alkyne **28**, which was prepared from 6-bromo-2-aminopyridine and trimethylsilylacetylene, produced intermediate **29a−b**. Raney nickel-mediated hydrogenation of **29a−b** yielded reduced product **30a−b**. Finally, the protecting groups on the aminopyridine rings were removed using microwave conditions to yield products **7** and **8**. A portion of intermediate **30b** was protected with Boc and then injected onto an OD-H chiral HPLC column to separate the enantiomers. Each enantiomerically pure compound was deprotected via microwave-assisted acidic hydrolysis to give optically active enantiomers **8S** and **8R**. Our diverse approach for the chiral resolution of the final deprotected compound (**8**) using CrownPak CR-(+), Chiralcel OD-RH, and Whelk-O 1 chiral reverse phase HPLC columns, and a Chiralcel OD-H chiral normal phase column with DEA, were not successful. Chiral derivatization of the final compound using Mosher's acid chloride, (S)-camphanyl chloride, and (S)-

mandelic chloride also were not successful because the molecules have multiple reactive amines.

RESULTS AND DISCUSSION

In Vitro Inhibitory Assays. The NOS isoform assays involved subjecting **3−8** to an oxyhemoglobin NO capture assay using a Biotek Gen5 microplate reader. IC_{50} values for each compound were determined in duplicate or triplicate using dose−response curves with nine concentration points (1 pM−3 mM). The standard deviation of the assays were less than 15% with nNOS or iNOS and less than 25% with eNOS. The inhibition constants (K_i) of these compounds were determined from the IC_{50} and K_m values (rat nNOS = 1.3 μM; murine iNOS = 8.2 μM; and bovine eNOS = 1.7 μM) for all three NOS isoforms using the following relationship: $K_i =IC_{50}/(1 + [S]/K_M)$

The selectivity of antagonism of nNOS relative to iNOS or eNOS was determined by calculating the ratios of the K_i values with iNOS or eNOS to those with nNOS. Compounds **3−8**, having various amino functional groups, were found to have moderate to excellent selectivity (50−2822 of e/n, 36−273 of

i/n) and moderate to good binding affinity (24−4370 nM) to nNOS. All of the synthesized molecules as well as three reference molecules (**31**, **32**, and **2**; for comparative purpose) and their associated activities are shown in Tables 1 and 2.

The compounds with an α-amino (or a hydroxyl) group and symmetric double heads, **3S**, **3R**, and **4**, exhibited about a 100 nM binding affinity to nNOS and modest selectivity against eNOS and iNOS, whereas **5R** and **5S**, having α-amino tailed asymmetric double heads, showed poor potency. Compounds **6−8**, having an α-aminomethyl tail with two aminopyridine head groups, showed improved potency by 1- to 5-fold. The orientation of the nitrogen on the middle aromatic ring was important; compound **7** was a relatively poor inhibitor of nNOS when the nitrogen was located in the narrow arc of the middle ring. Although the α-aminomethyl derivatives **6**, **7**, and **8** did not display improved binding affinity for nNOS compared with that of their parent molecules **31**, **32**, and **2**, it is noteworthy that all of those α-aminomethyl derivatives have better selectivity (Table 1) against iNOS and eNOS. In general, the α-aminomethyl derivatives are 2- to 3-fold (i/n) and 3- to 10-fold (e/n) more selective than their parent molecules. To further explore the inhibition potency and selectivity of racemic **8**, each enantiomer was prepared and assayed with the three NOS isoforms. Compound **8R**, the (*R*)-enantiomer of **8**, showed excellent potency (K_i = 24 nM) for nNOS with a 273-fold selectivity over iNOS and a 2822-fold selectivity over eNOS, the best in the series.

We also assayed compound **8** against human nNOS to explore whether the interactions are acceptable for the human isoform as well. Human nNOS is very similar to rat nNOS, except that the hydrophobic pocket surrounded by Met341, Leu337, and Tyr706 in rat nNOS is replaced by Met340, His342, and Tyr711. This pocket is where the second headgroup of this series of double-headed inhibitors fits. The inhibitory potency of **8** for human nNOS is 90 nM, similar to that (70 nM) of compound **1**,[25] which is our most potent human nNOS inhibitor with potential selectivity over human iNOS and eNOS.

Structure−Activity Relationship Studies. To aid in the structure−activity relationship studies for the series of double-headed aminopyridine compounds, we first determined the crystal structures of nNOS in complex with **3S**, **3R**, **4**, and **5** that bear an α-amino group (Table 1). Both **3S** and **3R** are able to bind to nNOS with both aminopyridine heads involved in H-bonds, one with Glu592 and the other with the propionate of the heme D-ring, respectively (Figure 3). In contrast, the parent compound (**31**) showed only one aminopyridine H-bonded with Glu592, while the rest of the inhibitor was badly disordered in structure (unpublished data). Introducing an α-amino group next to the center phenyl ring in **3S** and **3R** helps to stabilize the double-headed binding. Interestingly, the binding orientation of **3** is dependent on the chirality leading to different positions for the α-amine. The α-amino group of **3S** is next to the aminopyridine that H-bonds with Glu592 and points downward to the heme (Figure 3A), while the α-amino group of **3R** is on the side of the aminopyridine that H-bonds with the propionate of the heme D-ring (Figure 3B). This amino group can H-bond with a conserved water molecule that is bridging between the H_4B and the propionate of heme A-ring rather than replace the water as expected from modeling.

When the α-amino group is replaced with a hydroxyl group in **4**, the compound can no longer achieve a double-headed binding (Figure 3C). Instead, the aminopyridine next to the

hydroxyl group forms H-bonds with Glu592 so that the hydroxyl points toward the heme, similar to the position of the amino group in **3S**, but the second aminopyridine is partially disordered, hanging in the active site access channel and making only van der Waals contacts with the protein.

The structure of nNOS complexed with **5** was also checked to explore the binding mode for the compound bearing asymmetric double head groups. As expected, only the aminopyridine is able to anchor the inhibitor above the heme via H-bonds with Glu592, while the 4-methylpyridine head is poorly defined in the active site access channel (Figure 3D). Although a racemic mixture of **5S** and **5R** was used in crystal soaking, only the **5S** enantiomer was picked up by the nNOS in the crystal, which agrees with the better affinity of **5S** compared to that of **5R** (Table 1). The α-amino nitrogen is also able to H-bond with Glu592, which forces the center phenyl ring to bend toward the heme, causing a distortion of the propionate of the heme D-ring. Both the α-amino group and the amino-pyridine ring in **5S** wrap around the Glu592 side chain, which resembles the binding mode of the substrate, L-Arg, where the α-amino and guanidinium groups embrace Glu592. Note that the α-amino group from the same *S*-chiral centers of **3S** and **5S** ends up with two totally different positions, H-bonding either with a water molecule (**3S**) or with the heme D-ring propionate (**5S**), because the binding orientation of **3S** and **5S** is flipped by 180° relative to each other.

Both **3S** and **5S** showed modest isoform selectivity for nNOS over eNOS. We, therefore, also determined the crystal structures of **3S**, **3R**, and **5S** bound to eNOS. In the eNOS-**3S** structure (data not shown), only one aminopyridine was visible in the electron density that H-bonds with Glu363; the rest of **3S** was disordered, which prevented us from obtaining a fully refined structure. Nevertheless, double-headed binding, as seen in the nNOS-**3S** structure, can be ruled out because the Tyr477 side chain still H-bonds with the propionate of the heme D-ring, thus blocking the access of the second aminopyridine to the site. The one-headed binding of **3S** results in its poorer affinity to eNOS, leading to ~500-fold selection for nNOS over eNOS (Table 1). In contrast, **3R** binds to eNOS in a bouble-headed mode, as seen in Figure 4A, which is almost no different from what is observed in the nNOS-**3R** structure (Figure 3B), thus giving 5-fold improved affinity to eNOS compared with that of **3S** (Table 1). Although having a similar binding mode to both nNOS and eNOS, **3R** still shows 118-fold better affinity to nNOS than eNOS. Below, we discuss in more detail what gives rise to the isoform selection when the binding mode for an inhibitor is identical in the two isoforms.

The structure of eNOS-**5S** shows some intriguing features (Figure 4B). While the aminopyridine makes H-bonds with Glu363, which is the same as that seen in the nNOS-**5S** structure, the α-amino group does not directly H-bond with Glu363. Instead, a water molecule is bridging in between. This binding preference resembles what we have observed for some nNOS selective dipeptide amide inhibitors, where the α-amino group of the dipeptide inhibitor made a direct H-bond with Glu592 in nNOS but was bridged by a water molecule in between the α-amino of the inhibitor and Glu363 in eNOS.[26] This different binding preference results from the better electrostatic stabilization that the α-amino group of the inhibitor experiences by its proximity next to two negatively charged residues, Glu592 and Asp597 in nNOS, compared with just one negatively charged residue, Glu363 and Asn368 in eNOS. Therefore, the loss of the electrostatic interactions in
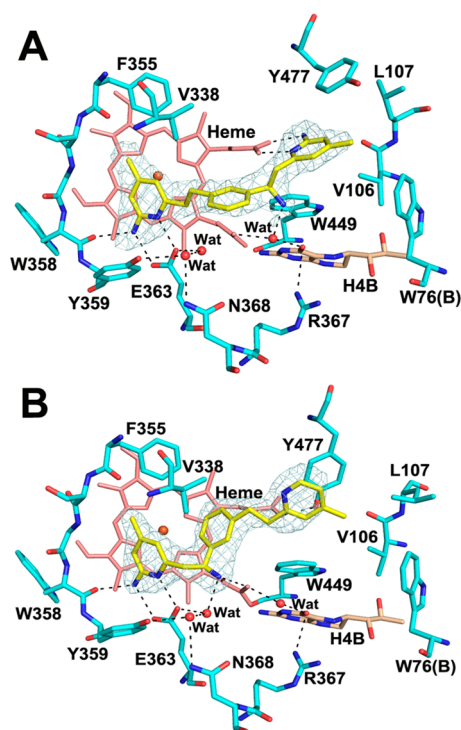
Figure 4. Active site structures of bovine eNOS in complex with (A) **3R** (PDB: 4CTY) and (B) **5** or **5S** (PDB: 4CTZ). The $F_o - F_c$ omit electron density for the inhibitor is displayed at the 2.5 σ contour level. The major H-bonds are depicted with dashed lines.

eNOS explains the 363-fold selectivity observed for **5S** (Table 1).

The double-headed compounds with only an α-amino group on the side chain (**3S**, **3R**, **4**, and **5S**) do not quite reach the position of the pyrroline amine of parent compound **1** that can replace a water molecule (Figure 1B). This might be why the low nanomolar affinity and good isoform selectivity of **1** had not been achieved with **3−5**. We, therefore, introduced an aminomethyl group to racemic compounds **6**, **7**, and **8** (Figure 2). We also designed three different center aromatic rings to further explore the influence of the polarity of this ring to the potency and selectivity of inhibitors. The inhibitory assays indicated that **6** and **8** indeed have improved potency (Table 1). The crystal structures of **6** and **8** bound to nNOS showed that they share a similar double-headed binding mode (Figure 5). Although the racemic samples were used for crystal preparation, the resulting structures were dominated by the R-enantiomer in both cases. The structure of nNOS-**6R** (Figure 5A) overlays well with that of nNOS-**3R** (Figure 3B) except that the aminomethyl group of **6** replaces a water molecule, thereby allowing it to make H-bonds with both the H4B and the propionate of heme A-ring, as was expected from the design. The better interactions from the aminomethyl group of **6** to both the H4B and the propionate afford a 2-fold improvement in potency compared with that of **3** (Table 1).

Compound **8** exhibits even better potency with nNOS than does **6** (Table 1), which may result from the extra nitrogen on the center pyridine ring of **8** (Figure 5B) versus the phenyl ring in **6** (Figure 5A). This pyridine ring in **8** is pulled a bit further up toward Asp597 in nNOS than is the phenyl ring of **6**, making water bridged H-bonds with the acidic residue and another weak H-bond (3.4 Å) with Gln478 (Figure 5B). We have also designed compound **7**, having the pyridine nitrogen
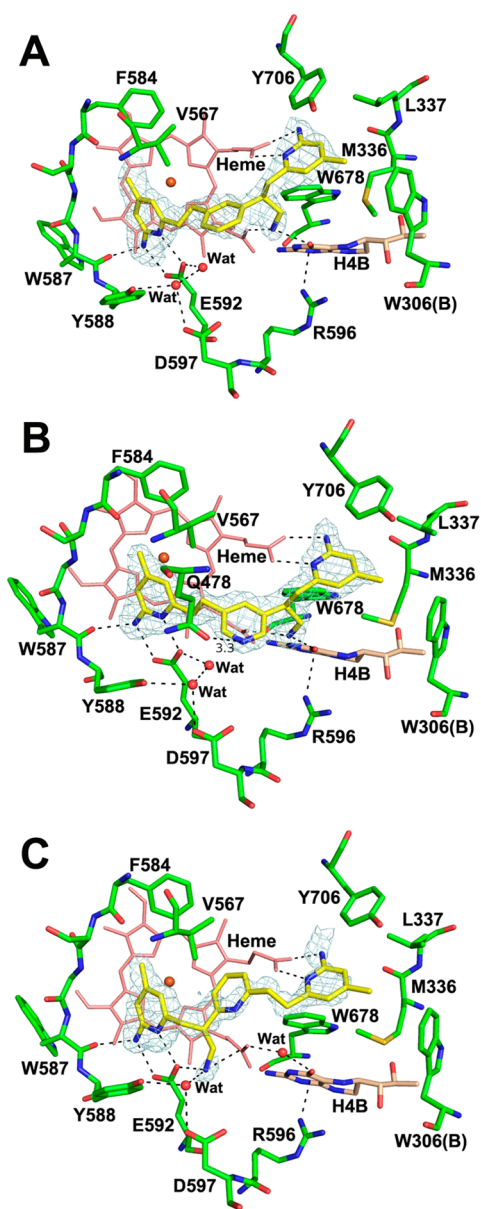

Figure 5. Active site structures of rat nNOS in complex with (A) **6** (PDB: 4CTU), (B) **8** or **8R** (PDB: 4CTW), and (C) **7** or **7S** (PDB: 4CTV). The $F_o - F_c$ omit electron density for the inhibitor is displayed at the 2.5 σ contour level. The major H-bonds are depicted with dashed lines. The weak H-bond in nNOS-**8R** is labeled with a distance in Å.

at an ortho-position relative to the other two substituents in contrast to the meta-position in **8**. To our surprise, **7** binds to nNOS (Figure 5C) in an orientation that is 180° flipped from that of **8** (Figure 5B). Moreover, it is the S-enantiomer of **7** that populates the structure, even though a racemic mixture of **7** was used in crystal preparation. In this binding orientation, the aminomethyl group of **7** makes a tight H-bond with Glu592. The positions of the neighboring aminopyridine, H-bonding to Glu592, and the center phenyl ring, bending toward the heme, overlay well with their counterparts in **5S** (Figure 3D). In addition, the second aminopyridine of **7** can also reach the site of the heme D-ring propionate in a double-headed mode (Figure 5C). Although in this flipped binding orientation, **7** shows poorer potency than **6** or **8**, it does have an impressive isoform selectivity (Table 1). We have tried, but failed, to get

an eNOS-**7** structure because the inhibitor was badly disordered except for the aminopyridine that H-bonds with Glu363 (data not shown). From the known structure of eNOS-**5S** (Figure 4B), we reasoned that the poor binding affinity of **7** toward eNOS must result from its inability to establish direct H-bonds with Glu363 by its aminomethyl group because of the more electropositive environment of Glu363 and Asn368 in eNOS, which would not allow a positively charged amino-methyl group to enter the pocket.

Compound **8** exhibits the best potency toward nNOS in the series, which prompted us to further explore the effects of chirality on the inhibitory potency and selectivity. Enantiopure **8S** and **8R** were synthesized, and crystal structures of both enantiomers bound to nNOS and eNOS were determined. Indeed, **8R** gives the best potency (24 nM) with nNOS and 2822-fold selectivity for nNOS over eNOS (Table 2). Both **8S** and **8R** show very similar double-headed binding to nNOS; the nNOS-**8R** structure is the same as that of nNOS-**8** (Figure 5B), while the nNOS-**8S** structure (Figure 6A) can be, more or less, superimposed on nNOS-**8R**, with the only exception being around the chiral center. Also, the center pyridine of **8S** can make a better H-bond (2.9−3.0 Å) with Gln478. Regardless of the chirality, the aminomethyl group in both **8S** and **8R** can replace a water molecule equally well, thus making direct H-bonds with both the H$_4$B and the propionate of the heme D-ring. The similarity in structure seems to be reasonable considering the ∼3-fold difference in potency between **8S** and **8R**. The eNOS-**8S** structure (Figure 6B) shows a one-headed binding mode since the access to the heme D-ring propionate from the second aminopyridine of **8S** is blocked by the Tyr477 side chain, which remains in its position, H-bonding with the same propionate. Therefore, the second aminopyridine group is poorly defined in structure, although the first aminopyridine and aminomethyl groups maintain the H-bonding interactions that are also observed in nNOS-**8S** (Figure 6A). To our surprise, we found no significant difference in the binding mode of **8R** to eNOS (Figure 6C) versus that to nNOS (Figure 5B). With a double-headed binding mode, the center pyridine of **8R** in eNOS points toward the direction of Asn368, just like its counterpart in nNOS, which points toward Asp597. In contrast, the central pyridine ring of **8S** in eNOS, in a one-headed binding, bends away from Asn368 and makes a better H-bond with Gln249 (Figure 6B). This may be part of the reason that **8S** binds better to eNOS than does **8R** (Table 2).

The structural binding mode alone cannot explain the 2822-fold isoform selectivity of **8R** for nNOS over eNOS. This is not the first time that a highly selective NOS inhibitor shows an almost identical binding mode to nNOS and eNOS. The previous examples were parent compound **1**[22] and its amino-analogue.[24] To better understand the basis for isoform selectivity, we turned to a computational approach that proved useful in previous studies with NOS inhibitors.[24] Using the MM-PBSA approach, we first calculated the ΔG for **8R** bound to nNOS. The value from this calculation is called PB$_{total}$ and includes the solvation and enthalpic terms but not the decrease in entropy upon inhibitor moving from solution to the active site. Since we are examining exactly the same inhibitor binding to nNOS and eNOS, ignoring this entropic contribution introduces little error. Table 3 provides the results of the MM-PBSA calculations.

This approach comes to within 0.8 kcal/mol of estimating the ΔG of binding to eNOS and also shows that the primary difference between eNOS and nNOS is the more favorable
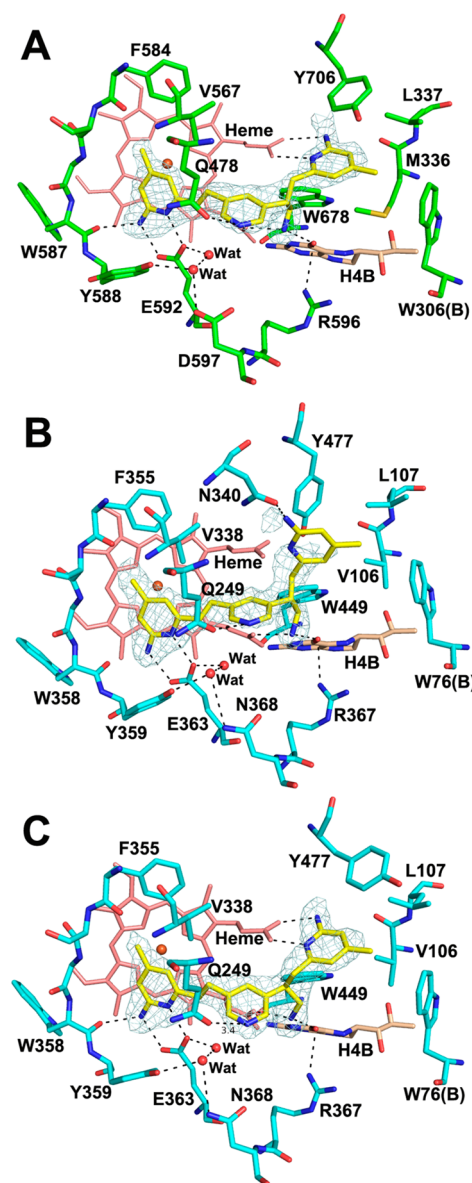

Figure 6. Active site structures of rat nNOS in complex with (A) **8S** (PDB: 4CTX) and of bovine eNOS with (B) **8S** (PDB: 4CU1) and (C) **8R** (PDB: 4CU0). The $F_o − F_c$ omit electron density for inhibitor is displayed at 2.5 σ contour level. The major H-bonds are depicted with dashed lines. The weak H-bond in eNOS-**8R** is labeled with a distance in Å.

Table 3. Results of the MM-PBSA Calculations (kcal/mol)

protein	ELE	VDW	PB$_{ele}$	PB$_{total}$	ΔG_{calc}	ΔG_{exp}
nNOS	−1018.7	−44.92	−41.1	−92.2	−10.4[a]	−10.4
eNOS	−818.7	−41.82	−9.57	−57.51	−6.5	−5.7

[a]ΔG_{calc} for nNOS was normalized to match ΔG_{exp} by dividing PB$_{total}$ by ΔG_{exp} and then using this conversion factor to compute ΔG_{clac} for eNOS. ELE and VDW are the electrostatic and van der Waals contributions, respectively, to inhibitor binding. PB$_{ele}$ is the sum of ELE and the reaction field energy calculated with the Poisson−Boltzmann equation and thus represents the total electrostatic component of inhibitor binding. PB$_{total}$ is the sum of all energies and represents the total free energy of binding uncorrected for the entropic contribution of the inhibitor moving from solution to the active site.

electrostatic interactions between the inhibitor and nNOS than those in eNOS. We attribute this primarily to Asp597 in nNOS vs Asn368 in eNOS, even though Asp597 does not directly contact the inhibitor. If the active site pocket exhibits a relatively low dielectric milieu, then long-range electrostatic stabilization by Asp597 on both the aminomethyl group and the central pyridine of **8R** could be quite substantial. However, when the binding of **8R** to eNOS is forced into the same double-headed mode as that with nNOS, the penalty toward electrostatic interactions leads to poorer binding and, therefore, higher isoform selectivity.

■ CONCLUSIONS

A series of α-amino functionalized aminopyridine derivatives (**3−8**) were designed based on the comparison and rationale that the pyrrolidine of lead **1**, interacting with a heme propionate and H$_4$B, is the key to isoform selectivity. Therefore, an α-amino or aminomethyl group has been installed in the other lead (**2**) to probe the structure−selectivity relationship, while providing a substantially simple scaffold that retains selectivity (Figure 1). In general, the symmetric double-headed aminopyridine compounds (**3** and **4**) showed better potency than the asymmetric one (**5**) because the former can establish H-bonds through both head groups. Although a simple α-amino group installed on the side chain can stabilize the double-headed inhibitor binding mode, only the amino-methyl group is long enough to reach a water site. By replacing the water molecule, the inhibitor is able to make H-bonds with both the H$_4$B and the propionate of the heme A-ring. These interactions seem to be crucial to gain the isoform selectivity for the inhibitors. Compound **8R**, the best inhibitor discovered in this study, exhibits excellent nNOS potency (24 nM) and isoform selectivity (273-fold for i/n and 2822-fold for e/n). It also showed <100 nM potency for human nNOS. However, the crystal structures of **8R** complexed with nNOS and eNOS share an almost identical binding mode, which is similar to what was observed with parent compound **1**.[22] A free energy calculation indicated that the different electrostatic environments in the active site of the two NOS isoforms give rise to the isoform distinct binding affinity, even for inhibitors that exhibit the same binding mode. The knowledge gained by this study will provide the basis for the design of further novel and isoform-selective inhibitors.

■ EXPERIMENTAL SECTION

Materials, Synthetic Methods, and Molecular Characterization. All starting reagents and solvents were purchased from Sigma-Aldrich, TCI America, and Matrix Scientific and were used without further purification. Solvents were purified by passage through a solvent column composed of activated alumina and a supported copper redox catalyst. Moisture or oxygen-sensitive reactions were performed under an atmosphere of dry N$_2$ or argon. A Biotage Initiator microwave system was used for microwave-assisted reactions. Thin-layer chromatography was carried out on E. Merck precoated silica gel 60 F254 plates. An Agilent 971-FP flash purification system with various SiliaSep (Silicycle, 40−63 μm, 60 Å) prepacked silica gel cartridges was used for flash column chromatography. ^{1}H NMR and ^{13}C NMR spectra were recorded in the indicated solvent on a Bruker Avance-III (500 and 126 MHz for ^{1}H and ^{13}C, respectively) spectrometer. Chemical shifts are reported as δ values in parts per million downfield from TMS (δ 0.0) as the internal standard in CDCl$_3$. MS was performed on a system consisting of an electrospray ionization (ESI) source in a Thermo Finnigan LCQ and Bruker amaZon SL mass spectrometer. High-resolution mass spectra were obtained using an Agilent 6210 LC-TOF spectrometer. The purity of

the compounds was evaluated on an Beckman Gold reverse phase analytical HPLC system using an Phenonemex Gemini C-18 (4.6 × 250 mm, 5 μm) or Luna C-8 (4.6 × 250 mm, 5 μm) reverse phase columns with UV absorbance and evaporative light scattering detection. Purities of all compounds that were subjected to the biological assay were >95%. The direct chiral resolutions of racemic **8R** and **8S** were performed on a Beckman Gold HPLC system using a Chiralcel OD-H HPLC column (Daicel, 250 × 4.6 mm i.d., 5 mm). Hexanes and isopropanol (85−92% hexanes) were used as the mobile phases. The operation temperature was 25 °C, and the flow rate was 0.8 mL/min with 254 nm UV detection. Optical rotations were measured on a PerkinElmer Model 341 digital readout polarimeter.

General Procedure for the Deprotection of 2-(2,5-Dimethyl-1H-pyrrol-1-yl)pyridine Derivatives Using Microwave Irradiation:[27] Method A. To a 5 mL microwave vial equipped with a magnetic stir bar was added the protected aminopyridine (1.0 mmol), ethanol (2.5 mL), and concentrated hydrochloric acid (0.5 mL). After being capped, the vial was shaken vigorously and then heated in the microwave irradiator for 20 min at 120 °C (as recorded via the IR sensor of the microwave instrument). After being cooled to room temperature, the reaction mixture was concentrated in vacuo and purified by flash column chromatography using a SiliaSep C18 flash cartridge (25g, 40−63 μm/230−400 mesh, pore size 60 Å) with 5 to 80% MeOH in water as the mobile phase.

(S)-6-(2-Amino-2-(3-(2-(6-amino-4-methylpyridin-2-yl)ethyl)phenyl)ethyl)-4-methylpyridin-2-amine (3S) and (R)-6-(2-Amino-2-(3-(2-(6-amino-4-methylpyridin-2-yl)ethyl)phenyl)ethyl)-4-methylpyridin-2-amine (3R). The title compounds were synthesized using general method A. **3S** (55 mg, 58%) was prepared as a pale yellow gel from **13a** (180 mg, 0.26 mmol), and **3R** (50 mg, 60%) was prepared as a pale yellow gel from **13b** (160 mg, 0.23 mmol). **3S**, $[\alpha]^{20}_D$ = +72.1° (c 3 g/L, MeOH); **3R**, $[\alpha]^{20}_D$ = −79.2° (c 2 g/L, MeOH). ^{1}H NMR (500 MHz, MeOD) δ 7.22−7.17 (m, 1H), 7.14 (qt, J = 2.9, 1.9, 1.4 Hz, 2H), 7.05 (dt, J = 7.4, 1.6 Hz, 1H), 6.25 (s, 1H), 6.24 (ss, 2H), 6.18 (s, 1H), 4.21 (t, J = 7.1 Hz, 1H), 2.89 (dd, J = 9.6, 6.4 Hz, 2H), 2.81 (d, J = 7.1 Hz, 2H), 2.79−2.71 (m, 2H), 2.13 (s, 3H), 2.11 (s, 3H); ^{13}C NMR (126 MHz, MeOD) δ 160.86, 160.70, 159.73, 157.35, 151.03, 150.86, 145.85, 143.10, 129.46, 128.35, 127.82, 125.18, 115.89, 114.67, 108.22, 107.92, 57.15, 48.09, 40.64, 37.32, 21.08, 21.05. HRMS (ESI): calcd for C$_{22}$H$_{28}$N$_5$ [M + H]$^+$, 362.2339; found, 362.2338.

(R)-6-(2-Amino-2-(3-(2-(4-methylpyridin-2-yl)ethyl)phenyl)ethyl)-4-methylpyridin-2-amine (5R) and (S)-6-(2-Amino-2-(3-(2-(4-methylpyridin-2-yl)ethyl)phenyl)ethyl)-4-methylpyridin-2-amine (5S). Method A was used to prepare **5R** (153 mg, 65%, colorless gel) from **19a** (360 mg, 0.682 mmol) and **5S** (22 mg, 60%, colorless gel) from **19b** (55 mg, 0.104 mmol). **5S**, $[\alpha]^{20}_D$ = −20.0° (c 2 g/L, MeOH); **5R**, $[\alpha]^{20}_D$ = +19.2° (c 2 g/L, MeOH). ^{1}H NMR (500 MHz, MeOD) δ 8.54 (d, J = 6.0 Hz, 1H), 7.79 (s, 1H), 7.68 (d, J = 5.9 Hz, 1H), 7.63 (s, 1H), 7.51−7.37 (m, 2H), 7.36−7.29 (m, 1H), 6.68 (s, 2H), 4.87 (d, J = 7.8 Hz, 1H), 3.51 (dd, J = 14.7, 7.9 Hz, 1H), 3.42−3.34 (m, 3H), 3.21−3.14 (m, 2H), 2.62 (s, 3H), 2.34 (s, 3H); ^{13}C NMR (126 MHz, MeOD) δ 162.50, 158.89, 156.51, 156.12, 143.95, 142.17, 141.24, 137.24, 131.02, 130.88, 129.16, 128.68, 127.00, 126.98, 116.76, 112.22, 55.32, 38.40, 35.76, 22.36, 21.96. HRMS (ESI): calcd for C$_{22}$H$_{27}$N$_4$ [M + H]$^+$, 347.2230; found, 347.2229.

6-(3-Amino-2-(3-(2-(6-amino-4-methylpyridin-2-yl)ethyl)phenyl)propyl)-4-methylpyridin-2-amine (6). Method A was used to prepare **6** (144 mg, 43%, pale yellow gel) from **24** (475 mg, 0.89 mmol). ^{1}H NMR (500 MHz, MeOD) δ 7.43 (s, 1H), 7.32 (t, J = 7.6 Hz, 1H), 7.21 (dt, J = 7.5, 1.8 Hz, 2H), 6.68 (s, 2H), 6.62 (s, 1H), 6.50 (s, 1H), 3.60−3.51 (m, 1H), 3.40−3.34 (m, 2H), 3.29 (dd, J = 14.3, 6.1 Hz, 1H), 3.07−3.00 (m, 5H), 2.38 (s, 3H), 2.28 (s, 3H); ^{13}C NMR (126 MHz, MeOD) δ 159.08, 158.70, 155.78, 150.00, 147.22, 142.47, 139.40, 130.61, 129.59, 129.31, 127.58, 116.07, 114.88, 111.16, 110.83, 44.87, 44.69, 37.99, 35.93, 35.61, 22.01, 21.91. HRMS (ESI): calcd for C$_{23}$H$_{30}$N$_5$ [M + H]$^+$, 376.2496; found, 376.2502.

6-(3-Amino-2-(6-(2-(6-amino-4-methylpyridin-2-yl)ethyl)pyridin-2-yl)propyl)-4-methylpyridin-2-amine (7). Method A was used to prepare **7** (87 mg, two step 43%, pale yellow gel) from crude **30a** (300 mg). ^{1}H NMR (500 MHz, MeOD) δ 7.83 (m, 1H), 7.38 (m, 1H), 7.33 (m, 1H), 6.73 (s, 1H), 6.70 (s, 1H), 6.65 (s, 1H), 6.45 (s, 1H),

3.80 (s, 1H), 3.61 (dd, J = 12.9, 9.0 Hz, 1H), 3.37 (t, J = 4.7 Hz, 1H), 3.23 (m, 6H), 2.39 (s, 3H), 2.29 (s, 3H); ^{13}C NMR (126 MHz, MeOD) δ 160.66, 159.10, 158.71, 157.66, 155.90, 155.79, 149.94, 146.66, 124.54, 124.02, 115.82, 114.76, 111.48, 110.92, 44.82, 43.32, 37.01, 36.55, 32.91, 21.99, 21.89. HRMS (ESI): calcd for $C_{22}H_{29}N_6$ [M + H]$^+$, 377.2448; found, 377.2455.

(S)-6-(3-Amino-2-(5-(2-(6-amino-4-methylpyridin-2-yl)ethyl)-pyridin-3-yl)propyl)-4-methylpyridin-2-amine (8S) and *(R)-6-(3-Amino-2-(5-(2-(6-amino-4-methylpyridin-2-yl)ethyl)-propyl)-4-methylpyridin-2-amine (8R).* Method A was used to prepare **8** (45 mg, 41%) from racemic **30b** (180 mg), **8S** (21 mg, 69%) from enantiomer **30c-1** (43 mg), and **8R** (15 mg, 79%) from enantiomer **30c-2** (32 mg). **8S**, $[\alpha]^{20}_D$ = −85.3° (c 4 g/L, MeOH); **8R**, $[\alpha]^{20}_D$ = +84.9° (c 3 g/L, MeOH). ^{1}H NMR (500 MHz, MeOD) δ 8.44 (s, 2H), 8.20 (d, J = 2.2 Hz, 1H), 6.74 (s, 1H), 6.71 (s, 1H), 6.65 (s, 1H), 6.58 (s, 1H), 3.75−3.66 (m, 1H), 3.50 (dd, J = 13.1, 9.9 Hz, 1H), 3.42 (dd, J = 13.1, 5.3 Hz, 1H), 3.39−3.34 (m, 1H), 3.13 (td, J = 9.8, 9.4, 5.6 Hz, 5H), 2.39 (s, 3H), 2.31 (s, 3H); ^{13}C NMR (126 MHz, MeOD) δ 159.12, 158.75, 155.95, 155.84, 149.33, 147.89, 146.49, 138.99, 138.68, 136.11, 116.10, 114.96, 111.51, 111.08, 44.14, 42.24, 37.57, 34.83, 32.89, 21.99, 21.89. HRMS (ESI): calcd for $C_{22}H_{29}N_6$ [M + H]$^+$, 377.2448; found, 377.2454.

2-(6-(2,5-Dimethyl-1H-pyrrol-1-yl)-4-methylpyridin-2-yl)-1-(3-(2-(6-(2,5-dimethyl-1H-pyrrol-1-yl)-4-methylpyridin-2-yl)ethyl)phenyl)-ethanol (11). To a solution of **9** (1.0 g, 5.0 mmol) in THF (25 mL) was added n-BuLi (1.6 M solution in hexanes, 3.12 mL, 5.0 mmol), and the reaction was stirred for 30 min at 0 °C. This mixture was transferred to a solution of 3-(bromomethyl)benzaldehyde (**10**, 396 mg, 2.0 mmol) in THF (25 mL) at −78 °C via a cannula. The reaction mixture was allowed to stir for an additional 20 min and then quenched with H$_2$O (50 mL). After the addition of ethyl acetate (50 mL), the organic layer was partitioned, dried with MgSO$_4$, and concentrated by rotary evaporation. The resulting yellow oil was purified by flash chromatography (EtOAc/hexanes) to yield 2,5-dimethylpyrrole-protected product **11** as a yellow oil (663 mg, 64%). ^{1}H NMR (500 MHz, CDCl$_3$) δ 7.33−7.25 (m, 3H), 7.14−7.09 (m, 1H), 6.99 (s, 1H), 6.95 (s, 2H), 6.89 (s, 1H), 5.93 (s, 2H), 5.91 (s, 2H), 5.15 (m, 1H), 3.17 (m, 2H), 3.10 (m, 4H), 2.42 (s, 3H), 2.40 (s, 3H), 2.18 (s, 6H), 2.16 (s, 6H); ^{13}C NMR (126 MHz, CDCl$_3$) δ 161.01, 159.29, 151.62, 151.13, 150.28, 149.53, 143.99, 141.63, 128.56, 128.50, 128.40, 127.51, 125.97, 123.52, 123.46, 122.67, 120.77, 120.10, 106.93, 106.68, 73.25, 45.73, 39.78, 36.64, 35.98, 24.72, 21.10, 13.31; MS (ESI) m/z 519.32 [M + H]$^+$.

2-(2-Azido-2-(3-(2-(6-(2,5-dimethyl-1H-pyrrol-1-yl)-4-methylpyridin-2-yl)ethyl)phenyl)ethyl)-6-(2,5-dimethyl-1H-pyrrol-1-yl)-4-methylpyridine (12). To a stirred solution of triphenylphosphine (314 mg, 1.2 mmol) and diethylazodicarboxylate (210 mg, 1.2 mmol) in dry THF (15 mL), diphenylphosphonyl azide (331 mg, 1.2 mmol) was added dropwise followed by a THF solution of **11** (518 mg, 1.0 mmol). After stirring for 1 h at room temperature, the reaction mixture was concentrated in vacuo and purified by flash column chromatography to yield the title compound (522 mg, 96%) as a colorless oil. ^{1}H NMR (500 MHz, CDCl$_3$) δ 7.30 (t, J = 7.9 Hz, 2H), 7.22−7.15 (m, 3H), 6.99 (s, 1H), 6.94 (s, 1H), 6.92 (s, 1H), 6.89 (s, 1H), 5.94 (s, 2H), 5.92 (s, 2H), 5.12 (t, J = 7.3 Hz, 1H), 3.16 (d, J = 7.4 Hz, 2H), 3.10 (s, 4H), 2.38 (s, 3H), 2.16 (ss, 12H); ^{13}C NMR (126 MHz, CDCl$_3$) δ 160.66, 157.25, 151.78, 151.67, 149.86, 149.52, 142.22, 139.42, 128.84, 128.52, 128.48, 126.94, 124.55, 123.86, 122.67, 120.85, 120.13, 106.80, 106.70, 65.75, 44.75, 39.66, 35.79, 21.05, 20.99, 13.29, 13.25; MS (ESI) m/z 544.21 [M + H]$^+$.

(1S,4S)-N-((S)-2-(6-(2,5-Dimethyl-1H-pyrrol-1-yl)-4-methylpyridin-2-yl)-1-(3-(2-(6-(2,5-dimethyl-1H-pyrrol-1-yl)-4-methylpyridin-2-yl)ethyl)phenyl)ethyl)-4,7,7-trimethyl-3-oxo-2-oxabicyclo[2.2.1]-heptane-1-carboxamide (13a) and *(1S,4S)-N-((R)-2-(6-(2,5-Dimethyl-1H-pyrrol-1-yl)-4-methylpyridin-2-yl)-1-(3-(2-(6-(2,5-dimethyl-1H-pyrrol-1-yl)-4-methylpyridin-2-yl)ethyl)phenyl)ethyl)-4,7,7-trimethyl-3-oxo-2-oxabicyclo[2.2.1]heptane-1-carboxamide (13b).* To the solution of **12** (500 mg, 0.92 mmol) in THF (25 mL) was added dropwise a 1.0 M solution of LiAlH$_4$ in THF (1.4 mL, 1.4 mmol) at 0 °C. After being stirred for 3 h at the same temperature, the reaction mixture was allowed to warm to room temperature, and the reaction

was quenched by sequential addition of i-PrOH (1 mL), water (15 mL), and then 1 M NaOH aq (10 mL). The organic materials were extracted with ethyl acetate (25 mL) three times, and the combined organic layers were washed with brine, dried over anhydrous MgSO$_4$, and then concentrated in vacuo to yield a crude amine (2-(6-(2,5-dimethyl-1H-pyrrol-1-yl)-4-methylpyridin-2-yl)-1-(3-(2-(6-(2,5-di-methyl-1H-pyrrol-1-yl)-4-methylpyridin-2-yl)ethyl)phenyl)ethan-1-amine). To the solution of the produced amine in dichloromethane (25 mL) was added (*S*)-camphamic chloride (325 mg, 1.5 mmol) and triethylamine (0.279 mL, 2.0 mmol) at 0 °C. After being stirred for 12 h at room temp, the reaction mixture was quenched with H$_2$O (50 mL). After the addition of dichloromethane (25 mL), the organic layer was partitioned, dried with MgSO$_4$, concentrated by rotary evaporation, and purified by flash chromatography (EtOAc/hexanes) to yield diastereomeric pure compounds **13a** (180 mg, 28%) and **13b** (161 mg, 25%) as a pale yellow oil. **13a**: ^{1}H NMR (500 MHz, CDCl$_3$) δ 7.19 (t, J = 7.6 Hz, 1H), 7.14 (t, J = 1.8 Hz, 1H), 7.11 (dt, J = 7.6, 1.5 Hz, 1H), 7.06 (dt, J = 7.5, 1.4 Hz, 1H), 6.98 (d, J = 8.4 Hz, 1H), 6.93 (s, 1H), 6.92 (s, 1H), 6.84 (ss, 2H), 5.87 (s, 2H), 5.86 (s, 2H), 5.51 (td, J = 8.7, 5.8 Hz, 1H), 3.26 (dd, J = 14.0, 5.9 Hz, 1H), 3.17 (dd, J = 14.0, 9.0 Hz, 1H), 3.01 (q, J = 2.5, 1.8 Hz, 4H), 2.40 (ddd, J = 13.4, 10.4, 4.1 Hz, 1H), 2.36 (s, 3H), 2.31 (s, 3H), 2.11 (s, 6H), 2.06 (s, 6H), 1.90−1.73 (m, 2H), 1.61 (ddd, J = 12.7, 8.9, 4.2 Hz, 1H), 1.04 (s, 3H), 0.97 (s, 3H), 0.57 (s, 3H); ^{13}C NMR (126 MHz, CDCl$_3$) δ 178.24, 165.99, 160.78, 157.36, 151.82, 151.54, 149.74, 142.05, 141.27, 128.80, 128.51, 128.49, 127.75, 126.68, 124.04, 123.29, 122.58, 120.64, 120.12, 106.85, 106.73, 92.49, 55.28, 53.72, 53.23, 44.37, 39.63, 35.88, 30.27, 29.03, 21.04, 20.95, 16.61, 16.18, 13.36, 13.30, 9.72; MS (ESI) m/z 720.36 [M + Na]$^+$. **13b**: ^{1}H NMR (500 MHz, CDCl$_3$) δ 7.16 (t, J = 7.6 Hz, 1H), 7.14−7.09 (m, 2H), 7.06 (dd, J = 7.7, 1.6 Hz, 1H), 7.03 (dt, J = 7.6, 1.4 Hz, 1H), 6.89 (s, 2H), 6.84 (s, 2H), 5.87 (s, 2H), 5.84 (s, 2H), 5.44 (td, J = 8.2, 6.1 Hz, 1H), 3.27 (dd, J = 14.0, 6.1 Hz, 1H), 3.20 (dd, J = 14.0, 8.3 Hz, 1H), 2.98 (d, J = 2.0 Hz, 4H), 2.40−2.34 (m, 4H), 2.32 (s, 3H), 2.11 (s, 6H), 2.04 (s, 6H), 1.85 (ddd, J = 13.0, 10.8, 4.2 Hz, 1H), 1.67 (ddd, J = 13.0, 9.3, 4.1 Hz, 1H), 1.59 (ddd, J = 13.2, 9.3, 3.8 Hz, 1H), 1.04 (s, 3H), 0.98 (s, 3H), 0.74 (s, 3H); ^{13}C NMR (126 MHz, CDCl$_3$) δ 178.22, 166.28, 160.74, 157.33, 151.67, 149.73, 141.92, 141.45, 128.66, 128.49, 127.63, 126.64, 124.05, 123.42, 122.51, 120.77, 120.12, 106.75, 106.70, 92.30, 55.25, 54.01, 53.37, 43.95, 39.64, 35.87, 30.23, 29.06, 21.04, 21.01, 16.69, 16.43, 13.30, 13.24, 9.69; MS (ESI) m/z 720.37 [M + Na]$^+$.

3-(2-(4-Methylpyridin-2-yl)ethyl)benzonitrile (16). To a solution of **14** (0.804 g, 7.5 mmol) in dry THF (30 mL) was added n-BuLi (1.6 M solution in hexanes, 4.68 mL, 7.5 mmol), and the reaction was stirred for 30 min at 0 °C. This solution (red color) was added dropwise to a solution of 3-(bromomethyl)benzonitrile (**15**, 1.16 g, 6.0 mmol) in THF (20 mL) at −78 °C using a cannula, until the solution became pale red. The reaction mixture was allowed to stir for an additional 20 min and then quenched with H$_2$O (50 mL). After the addition of ethyl acetate (100 mL), the organic layer was partitioned, dried with MgSO$_4$, and concentrated in vacuo. The resulting yellow oil was purified by flash chromatography (EtOAc/hexanes) to yield the title compound as a yellow oil (680 mg, 51%). ^{1}H NMR (500 MHz, CDCl$_3$) δ 8.40 (d, J = 5.0 Hz, 1H), 7.52−7.39 (m, 3H), 7.36 (t, J = 7.6 Hz, 1H), 6.96 (dd, J = 5.1, 1.5 Hz, 1H), 6.89 (d, J = 1.6 Hz, 1H), 3.19−2.94 (m, 4H), 2.30 (s, 3H); ^{13}C NMR (126 MHz, CDCl$_3$) δ 159.85, 149.15, 147.57, 143.05, 133.15, 132.02, 129.78, 129.12, 123.96, 122.49, 119.04, 112.24, 39.44, 35.32, 20.97; MS (ESI) m/z 222.97 [M + H]$^+$.

3-(2-(4-Methylpyridin-2-yl)ethyl)benzaldehyde (17). To a solution of **16** (660 mg, 2.94 mmol) in dichloromethane (30 mL) was added 1.0 M solution of DIBAL in toluene (8.8 mL, 8.8 mmol) at 0 °C, and it was stirred for 3 h. The reaction mixture was then quenched with MeOH (3 mL) and water (25 mL). The mixture was warmed to ambient temperature, stirred for 30 min, and diluted with CH$_2$Cl$_2$ (50 mL). The organic layer was washed with Rochelle's solution and brine, dried over MgSO$_4$, and concentrated in vacuo. The resulting residue was purified by flash chromatography (EtOAc/hexanes) to yield the title compound as a yellow oil (350 mg, 53%). ^{1}H NMR (500 MHz, CDCl$_3$) δ 10.01 (s, 1H), 8.44 (d, J = 5.0 Hz, 1H), 7.77−7.68 (m, 2H),

7.52−7.42 (m, 2H), 6.98 (dd, J = 5.2, 1.6 Hz, 1H), 6.93 (s, 1H), 3.21−3.13 (m, 2H), 3.13−3.05 (m, 2H), 2.32 (s, 3H); ^{13}C NMR (126 MHz, CDCl$_3$) δ 192.58, 160.31, 149.17, 147.49, 142.80, 136.55, 134.81, 129.59, 129.03, 127.69, 123.94, 122.39, 39.79, 35.61, 21.00.

(S,E)-2-Methyl-N-(3-(2-(4-methylpyridin-2-yl)ethyl)benzylidene)-propane-2-sulfinamide (18). To a solution of (S)-*tert*-butanesulfina-mide (0.210 g, 1.7 mmol) in THF (5 mL) was added **17** (350 mg, 1.55 mmol) followed by Ti(OEt)$_4$ (0.70 g, 3 mmol). The reaction solution was stirred overnight at room temperature (16 h), and then the reaction was quenched by the slow addition of saturated aqueous NaHCO$_3$ (10 mL). The resulting mixture was diluted with EtOAc (20 mL) and filtered through Celite, and the Celite pad was washed with EtOAc (20 mL). The organic layers were partitioned, dried over MgSO$_4$, and concentrated in vacuo. The residue was purified by silica gel chromatography (EtOAc/hexanes) to give the title compound (361 mg, 71% yield) as a pale yellow solid. ^{1}H NMR (500 MHz, CDCl$_3$) δ 8.56 (s, 1H), 8.43 (d, J = 5.0 Hz, 1H), 7.70 (d, J = 1.6 Hz, 1H), 7.67 (dt, J = 6.9, 1.8 Hz, 1H), 7.43−7.34 (m, 2H), 6.96 (dd, J = 5.0, 1.6 Hz, 1H), 6.94 (s, 1H), 3.16−3.00 (m, 4H), 2.31 (s, 3H), 1.28 (s, 9H); ^{13}C NMR (126 MHz, CDCl$_3$) δ 162.85, 160.44, 149.12, 147.45, 142.62, 134.13, 132.75, 129.08, 128.98, 127.46, 123.95, 122.36, 57.77, 39.87, 35.75, 22.63, 20.99; MS (ESI) m/z 329.35 [M + H]$^+$.

(S)-N-((R)-2-(6-(2,5-Dimethyl-1H-pyrrol-1-yl)-4-methylpyridin-2-yl)-1-(3-(2-(4-methylpyridin-2-yl)ethyl)phenyl)ethyl)-2-methylpro-pane-2-sulfinamide (19a down, major) and (S)-N-((S)-2-(6-(2,5-Dimethyl-1H-pyrrol-1-yl)-4-methylpyridin-2-yl)-1-(3-(2-(4-methyl-pyridin-2-yl)ethyl)phenyl)ethyl)-2-methylpropane-2-sulfinamide (19b). To a solution of **9** (250 mg, 1.25 mmol) in dry THF (15 mL) was added *n*-BuLi (1.6 M solution in hexanes, 0.781 mL, 1.25 mmol), and the reaction was stirred for 30 min at 0 °C. This solution was added dropwise to a solution of sulfonamide (**18**, 350 mg, 1.07 mmol) in THF (15 mL) at −78 °C using a cannula. After being stirred for an additional 20 min, the reaction mixture was quenched with H$_2$O (20 mL) and diluted with EtOAc (25 mL). The organic layer was partitioned, dried with MgSO$_4$, and concentrated in vacuo. The resulting yellow oil was purified by flash chromatography (EtOAc/hexanes) to yield title compounds **19a** (367 mg, 65%) and **19b** (62 mg, 11%). The minor product (**19b**) eluted first. **19a**: pale brown oil; ^{1}H NMR (500 MHz, CDCl$_3$) δ 8.43 (dd, J = 4.9, 0.9 Hz, 1H), 7.25−7.17 (m, 3H), 7.14−7.09 (m, 1H), 6.97−6.94 (m, 2H), 6.88 (s, 1H), 6.87 (s, 1H), 5.89 (s, 2H), 4.92−4.82 (m, 1H), 4.33 (d, J = 4.8 Hz, 1H), 3.47−3.34 (m, 1H), 3.20 (dd, J = 13.9, 6.1 Hz, 1H), 3.02 (s, 3H), 2.35 (s, 3H), 2.32 (s, 3H), 2.08 (s, 6H), 1.10 (s, 9H); ^{13}C NMR (126 MHz, CDCl$_3$) δ 160.87, 158.06, 151.49, 149.57, 149.03, 147.43, 142.08, 141.84, 128.64, 128.44, 127.94, 127.34, 124.90, 123.91, 123.87, 122.24, 120.59, 106.67, 59.49, 56.09, 45.43, 40.14, 36.09, 22.47, 22.13, 21.01, 20.97, 13.26; MS (ESI) m/z 551.15 [M + H]$^+$. **19b**: pale brown oil; ^{1}H NMR (500 MHz, CDCl$_3$) δ 8.44 (d, J = 5.1 Hz, 1H), 7.30−7.19 (m, 3H), 7.15 (dt, J = 7.5, 1.6 Hz, 1H), 6.97 (dd, J = 5.1, 1.5 Hz, 1H), 6.95 (s, 1H), 6.94 (s, 2H), 5.88 (s, 2H), 4.76 (ddd, J = 9.3, 4.1, 1.9 Hz, 1H), 3.21−3.09 (m, 2H), 3.04 (p, J = 2.8 Hz, 4H), 2.40 (s, 3H), 2.33 (s, 3H), 2.14 (s, 6H), 1.09 (s, 9H); ^{13}C NMR (126 MHz, CDCl$_3$) δ 160.89, 158.28, 151.28, 150.35, 149.07, 147.41, 142.17, 141.93, 128.58, 128.48, 127.83, 127.62, 125.13, 123.89, 123.57, 122.25, 120.91, 106.50, 57.95, 55.45, 45.58, 40.14, 36.12, 22.59, 21.08, 21.03, 13.27; MS (ESI) m/z 551.22 [M + Na]$^+$.

3-(2-(6-(2,5-Dimethyl-1H-pyrrol-1-yl)-4-methylpyridin-2-yl)ethyl)-benzonitrile (20). The title compound (785 mg, 83%) was prepared according to a similar procedure described for the synthesis of **16** using *n*-BuLi (1.6 M, 2.34 mL, 3.75 mmol), **9** (750 mg, 3.75 mmol), and **15** (0.582 g, 3.0 mmol). Colorless oil; ^{1}H NMR (500 MHz, CDCl$_3$) δ 7.54−7.43 (m, 3H), 7.39 (d, J = 15.3 Hz, 1H), 6.93 (s, 1H), 6.91 (s, 1H), 5.92 (s, 2H), 3.22−3.00 (m, 4H), 2.40 (s, 3H), 2.14 (s, 6H); ^{13}C NMR (126 MHz, CDCl$_3$) δ 159.86, 151.76, 149.72, 142.92, 133.17, 132.00, 129.85, 129.18, 128.45, 122.69, 120.41, 119.00, 112.32, 106.77, 39.05, 35.05, 21.02, 13.26; MS (ESI) m/z 632.34 [2 M + H]$^+$.

3-(2-(6-(2,5-Dimethyl-1H-pyrrol-1-yl)-4-methylpyridin-2-yl)ethyl)-benzaldehyde (21). The title compound (615 mg, 78%) was prepared according to similar procedures described for the synthesis of **17** using DIBAL (1M, 7.5 mL, 7.5 mmol) and **20** (780 mg, 2.48 mmol). Pale yellow oil; ^{1}H NMR (500 MHz, CDCl$_3$) δ 10.00 (s, 1H), 7.79−7.69

(m, 2H), 7.52−7.42 (m, 2H), 6.94 (s, 1H), 6.90 (s, 1H), 5.92 (s, 2H), 3.19 (ddd, J = 8.4, 5.9, 2.1 Hz, 2H), 3.14 (ddd, J = 8.9, 6.0, 2.1 Hz, 2H), 2.39 (s, 3H), 2.14 (s, 6H); ^{13}C NMR (126 MHz, CDCl$_3$) δ 192.52, 160.27, 151.71, 149.62, 142.62, 136.56, 134.81, 129.50, 129.07, 128.46, 127.79, 122.68, 120.28, 106.73, 39.34, 35.33, 21.01, 13.27.

2-(2,5-Dimethyl-1H-pyrrol-1-yl)-4-methyl-6-(3-(2-nitrovinyl)-phenethyl)pyridine (22). Compound **21** (600 mg, 1.88 mmol), nitromethane (0.151 mL, 2.83 mmol), and triethylamine (0.524 mL, 3.76 mmol) were dissolved in dichloromethane and stirred at room temperature for 2 h. After the solvent was removed under reduced pressure, the organic residue was redissolved in dichloromethane and then mixed with acetyl chloride (0.134 mL, 3.76 mmol) and triethylamine (0.655 mL, 4.7 mmol). After being stirred at room temperature for 1 h, the mixture was concentrated in vacuo and purified by column chromatography to give the title compound (577 mg, 85%) as a yellow solid. ^{1}H NMR (500 MHz, CDCl$_3$) δ 8.00 (d, J = 13.7 Hz, 1H), 7.58 (d, J = 13.6 Hz, 1H), 7.45−7.34 (m, 4H), 6.97 (s, 1H), 6.91 (s, 1H), 5.92 (s, 2H), 3.14 (h, J = 3.0 Hz, 4H), 2.41 (s, 3H), 2.15 (s, 6H); ^{13}C NMR (126 MHz, CDCl$_3$) δ 151.74, 149.66, 142.97, 139.23, 137.00, 132.50, 130.11, 129.45, 129.28, 128.47, 128.44, 126.97, 122.67, 120.31, 120.07, 106.79, 106.63, 39.36, 35.36, 21.03, 13.28, 13.25; MS (ESI) m/z 362.45 [M + H]$^+$.

2-(2,5-Dimethyl-1H-pyrrol-1-yl)-6-(3-(1-(6-(2,5-dimethyl-1H-pyr-rol-1-yl)-4-methylpyridin-2-yl)-3-nitropropan-2-yl)phenethyl)-4-methylpyridine (23). The title compound (531 mg, 61%) was prepared according to similar procedures described for the synthesis of **19a−b** using *n*-BuLi (1.6 M, 1.21 mL, 1.94 mmol), **9** (387 mg, 1.94 mmol), and **22** (560 mg, 1.55 mmol). Yellow oil; ^{1}H NMR (500 MHz, CDCl$_3$) δ 7.21 (t, J = 7.84 Hz, 1H), 7.09−7.02 (m, 3H), 6.90 (s, 1H), 6.89 (s, 1H), 6.88 (s, 2H), 5.92 (s, 4H), 4.74−4.57 (m, 2H), 4.12−4.02 (m, 1H), 3.15 (d, J = 7.69 Hz, 2H), 3.04 (s, 4H), 2.38 (s, 3H), 2.37 (s, 3H), 2.16 (s, 6H), 2.11 (s, 6H); ^{13}C NMR (126 MHz, CDCl$_3$) δ 160.60, 157.76, 151.80, 151.57, 149.94, 149.68, 142.17, 139.19, 128.90, 128.53, 128.47, 127.89, 127.66, 125.05, 123.37, 122.71, 120.84, 120.15, 106.83, 106.71, 79.79, 44.04, 41.34, 39.62, 35.77, 21.00, 20.99, 13.28, 13.24; MS (ESI) m/z 562.29 [M + H]$^+$.

3-(6-(2,5-Dimethyl-1H-pyrrol-1-yl)-4-methylpyridin-2-yl)-2-(3-(2-(6-(2,5-dimethyl-1H-pyrrol-1-yl)-4-methylpyridin-2-yl)ethyl)phenyl)-propan-1-amine (24). A solution of **23** (500 mg, 0.89 mmol) in EtOH (5 mL) and MeOH (5 mL) was stirred with Raney-Ni (50% in water, 0.4 mL) for 1 h at ambient temperature under a hydrogen atmosphere. The reaction mixture was filtered through Celite and concentrated in vacuo to yield the title compound (475 mg, 99%). ^{1}H NMR (500 MHz, CDCl$_3$) δ 7.22 (t, J = 7.9 Hz, 1H), 7.08−7.01 (m, 3H), 6.93 (s, 1H), 6.89 (s, 1H), 6.83 (ss, 2H), 5.91 (s, 2H), 5.90 (s, 2H), 3.21 (td, J = 7.9, 5.0 Hz, 1H), 3.13 (dd, J = 13.5, 7.4 Hz, 1H), 3.07−2.98 (m, 5H), 2.92 (qd, J = 12.9, 6.9 Hz, 2H), 2.39 (s, 3H), 2.33 (s, 3H), 2.15 (s, 6H), 2.10 (s, 6H). ^{13}C NMR (126 MHz, CDCl3) δ 160.93, 159.89, 151.63, 151.49, 149.51, 149.32, 142.58, 141.77, 128.60, 128.47, 128.43, 128.18, 126.78, 125.66, 123.35, 122.56, 120.20, 120.07, 106.71, 106.58, 49.54, 47.14, 42.21, 39.83, 35.94, 21.01, 20.96, 13.28, 13.20; MS (ESI) m/z 532.27 [M + H]$^+$.

2-Bromo-6-(2-nitrovinyl)pyridine (26a). The title compound (295 mg, 65%) was prepared according to a similar described for the synthesis of **22** using MeNO$_2$ (0.160 mL, 3.0 mmol) and **25a** (372 mg, 2.0 mmol). Yellow solid; ^{1}H NMR (500 MHz, CDCl$_3$) δ 8.05 (d, J = 13.07 Hz, 1H), 7.85 (d, J = 13.10 Hz, 1H), 7.67 (t, J = 7.71 Hz, 1H), 7.59 (dd, J = 0.92, 7.98 Hz, 1H), 7.45 (dd, J = 0.88, 7.45 Hz, 1H); ^{13}C NMR (126 MHz, CDCl$_3$) δ 150.37, 143.04, 141.72, 139.27, 135.26, 130.34, 125.09; MS (ESI) m/z 455.77 [2 M + H]$^+$.

3-Bromo-5-(2-nitrovinyl)pyridine (26b). The title compound (390 mg, 86%) was prepared according to a similar procedure described for the synthesis of **22** using MeNO$_2$ (0.160 mL, 3.0 mmol) and **25b** (372 mg, 2.0 mmol). Yellow solid; ^{1}H NMR (500 MHz, CDCl$_3$) δ 8.80 (d, J = 2.2 Hz, 1H), 8.74 (t, J = 2.7 Hz, 1H), 8.05 (t, J = 2.1 Hz, 1H), 7.97 (d, J = 13.8 Hz, 1H), 7.64 (d, J = 13.8 Hz, 1H); ^{13}C NMR (126 MHz, CDCl$_3$) δ 153.48, 148.10, 139.35, 137.53, 133.83, 128.15, 121.42; MS (ESI) m/z 455.98 [2 M + H]$^+$.

2-(2-(6-Bromopyridin-2-yl)-3-nitropropyl)-6-(2,5-dimethyl-1H-pyrrol-1-yl)-4-methylpyridine (27a). The title compound (329 mg,

60%) was prepared according to a similar procedure described for the synthesis of **19a−b** using *n*-BuLi (1.6 M, 1.00 mL, 1.60 mmol), **9** (320 mg, 1.60 mmol), and **26a** (290 mg, 1.28 mmol). Pale brown oil; ¹H NMR (500 MHz, CDCl₃) δ 7.43 (t, *J* = 7.67 Hz, 1H), 7.36 (d, *J* = 7.92 Hz, 1H), 7.10 (d, *J* = 7.40 Hz, 1H), 6.90 (s, 1H), 6.88 (s, 1H), 5.93 (s, 2H), 5.04 (dd, *J* = 9.68, 13.55 Hz, 1H), 4.66 (dd, *J* = 4.52, 13.58 Hz, 1H), 4.35−4.24 (m, 1H), 3.24 (dd, *J* = 7.27, 14.09 Hz, 1H), 3.19−3.07 (m, 1H), 2.38 (s, 3H), 2.13 (s, 6H); ¹³C NMR (126 MHz, CDCl₃) δ 160.51, 157.17, 151.93, 150.09, 142.07, 138.94, 128.43, 126.95, 123.59, 122.75, 120.94, 106.91, 106.84, 77.55, 44.24, 40.14, 21.00, 13.27; MS (ESI) *m/z* 450.96 [M + Na]⁺.

2-(2-(5-Bromopyridin-3-yl)-3-nitropropyl)-6-(2,5-dimethyl-1H-pyrrol-1-yl)-4-methylpyridine (27b). The title compound (375 mg, 51%) was prepared according to a similar procedure described for the synthesis of **19a−b** using *n*-BuLi (1.6 M, 1.34 mL, 2.15 mmol), **9** (430 mg, 2.15 mmol), and **26b** (390 mg, 1.72 mmol). ¹H NMR (500 MHz, CDCl₃) δ 8.59 (s, 1H), 8.42 (s, 1H), 6.92 (ss, 2H), 5.93 (s, 2H), 4.79 (dd, *J* = 13.1, 5.6 Hz, 1H), 4.70 (dd, *J* = 13.1, 9.2 Hz, 1H), 4.22 (dtd, *J* = 9.3, 7.6, 5.5 Hz, 1H), 3.23 (dd, *J* = 14.2, 7.7 Hz, 1H), 3.16 (dd, *J* = 14.2, 7.6 Hz, 1H), 2.39 (s, 3H), 2.10 (s, 6H); ¹³C NMR (126 MHz, CDCl₃) δ 156.39, 152.04, 150.42, 150.35, 147.36, 137.72, 136.59, 128.44, 123.47, 121.32, 120.94, 106.98, 78.82, 40.86, 40.55, 21.02, 13.25; MS (ESI) *m/z* 450.98 [M + Na]⁺.

2-(2,5-Dimethyl-1H-pyrrol-1-yl)-6-((6-(1-(6-(2,5-dimethyl-1H-pyrrol-1-yl)-4-methylpyridin-2-yl)-3-nitropropan-2-yl)pyridin-2-yl)-ethynyl)-4-methylpyridine (29a). The reaction mixture of **27a** (300 mg, 0.70 mmol), Pd(PPh₃)₂Cl₂ (23 mg, 0.035 mmol), CuI (6 mg, 0.035 mmol), PPh₃ (37 mg, 0.14 mmol), **28** (167 mg, 0.80 mmol), diethylamine (1.5 mL), and DMF (1.5 mL) were heated at 120 °C for 20 min in the microwave cavity. Then, the reaction mixture was treated with diethyl ether (20 mL), filtered, and concentrated in vacuo. The residue was purified by flash chromatography (EtOAc/hexanes) to give the title compound (306 mg, 78%) as a pale yellow oil. ¹H NMR (500 MHz, CDCl₃) δ 7.58 (t, *J* = 7.77 Hz, 1H), 7.53 (s, 1H), 7.47 (dd, *J* = 1.03, 7.76 Hz, 1H), 7.11 (d, *J* = 7.74 Hz, 1H), 7.08 (s, 1H), 6.90 (s, 1H), 6.85 (s, 1H), 5.93 (s, 2H), 5.91 (s, 2H), 5.16 (dd, *J* = 9.67, 13.66 Hz, 1H), 4.70 (dd, *J* = 4.66, 13.62 Hz, 1H), 4.33 (m, 1H), 3.26 (dd, *J* = 7.45, 14.02 Hz, 1H), 3.19 (dd, *J* = 7.75, 14.02 Hz, 1H), 2.49 (s, 3H), 2.36 (s, 3H), 2.18 (s, 6H), 2.13 (s, 6H); ¹³C NMR (126 MHz, CDCl₃) δ 159.78, 157.45, 152.39, 151.91, 150.01, 142.40, 141.88, 136.77, 128.57, 128.45, 127.37, 126.61, 123.82, 123.57, 123.00, 120.87, 106.95, 106.87, 88.03, 87.44, 44.65, 40.38, 20.98, 20.96, 13.28, 13.22; MS (ESI) *m/z* 559.24 [M + H]⁺.

2-(2,5-Dimethyl-1H-pyrrol-1-yl)-6-((5-(1-(6-(2,5-dimethyl-1H-pyrrol-1-yl)-4-methylpyridin-2-yl)-3-nitropropan-2-yl)pyridin-3-yl)-ethynyl)-4-methylpyridine (29b). The title compound (355 mg, 74%) was prepared using the same procedure described for the synthesis of **29a** from **27b** (370 mg, 0.86 mmol) and **28** (207 mg, 0.98 mmol). ¹H NMR (500 MHz, CDCl₃) δ 8.71 (s, 1H), 8.45 (s, 1H), 7.43 (s, 1H), 7.07 (s, 1H), 6.91 (ss, 2H), 5.92 (ss, 4H), 4.80 (dd, *J* = 13.0, 5.6 Hz, 1H), 4.71 (dd, *J* = 13.0, 9.2 Hz, 1H), 4.25 (m, 1H), 3.25 (dd, *J* = 14.2, 7.6 Hz, 2H), 3.16 (dd, *J* = 14.2, 7.7 Hz, 1H), 2.49 (s, 3H), 2.38 (s, 3H), 2.17 (s, 6H), 2.10 (s, 6H); ¹³C NMR (126 MHz, CDCl₃) δ 156.52, 152.43, 152.01, 151.80, 150.37, 150.09, 148.99, 141.78, 137.74, 134.50, 128.55, 128.46, 126.97, 123.47, 122.94, 121.27, 107.01, 106.93, 91.87, 85.09, 78.96, 40.96, 40.56, 21.02, 20.98, 14.23, 13.25, 13.22; MS (ESI) *m/z* 559.17 [M + H]⁺.

3-(6-(2,5-Dimethyl-1H-pyrrol-1-yl)-4-methylpyridin-2-yl)-2-(6-(2-(6-(2,5-dimethyl-1H-pyrrol-1-yl)-4-methylpyridin-2-yl)ethyl)pyridin-2-yl)propan-1-amine (30a). A solution of **29a** (300 mg, 0.54 mmol) in EtOH (5 mL) and MeOH (5 mL) was stirred with Raney-Ni (50% in water, 0.5 mL) for 7 h at ambient temperature under a hydrogen atmosphere. The reaction mixture was filtered through a PTFE membrane filter (diameter 25 mm, pore size 0.2 μm) and concentrated in vacuo to give the crude title compound (300 mg). ¹H NMR (500 MHz, MeOD) δ 7.50 (t, *J* = 7.7 Hz, 1H), 7.14 (s, 1H), 7.02 (d, *J* = 7.4 Hz, 1H), 6.99 (s, 1H), 6.97 (s, 1H), 6.95 (d, *J* = 7.5 Hz, 1H), 6.92 (s, 1H), 5.82 (s, 3H), 5.81 (s, 2H), 3.60−3.43 (m, 1H), 3.37 (s, 2H), 3.27−3.14 (m, 7H), 3.07 (dd, *J* = 12.9, 8.0 Hz, 1H), 2.93 (dd, *J* = 12.9, 5.4 Hz, 1H), 2.40 (s, 3H), 2.31 (s, 3H), 2.05 (s, 7H), 2.00 (s, 6H); ¹³C

NMR (126 MHz, MeOD) δ 162.44, 162.33, 161.77, 161.33, 152.85, 152.74, 152.53, 152.24, 138.13, 129.41, 129.39, 125.28, 124.53, 122.59, 122.34, 122.17, 122.12, 107.65, 107.57, 46.94, 41.38, 38.69, 38.12, 25.32, 20.97, 20.87, 13.25, 13.21; MS (ESI) *m/z* 533.19 [M + H]⁺.

3-(6-(2,5-Dimethyl-1H-pyrrol-1-yl)-4-methylpyridin-2-yl)-2-(6-(2-(6-(2,5-dimethyl-1H-pyrrol-1-yl)-4-methylpyridin-2-yl)ethyl)pyridin-2-yl)propan-1-amine (30b). The crude title compound (330 mg) was prepared using the same procedure described for the synthesis of **30a** from **27b** (350 mg, 0.63 mmol). ¹H NMR (500 MHz, CD₃Cl) δ 8.26 (s, 1H), 8.17 (s, 1H), 7.62 (s, 1H), 7.03 (s, 1H), 6.89 (s, 1H), 6.88 (s, 1H), 6.79 (s, 1H), 5.87 (s, 2H), 5.80 (s, 2H), 3.80−3.71 (m, 1H), 3.54−3.44 (m, 1H), 3.24−3.14 (m, 1H), 3.10−2.95 (m, 4H), 2.96−2.77 (m, 2H), 2.39 (s, 3H), 2.27 (s, 3H), 2.09 (s, 6H), 1.99 (s, 6H); ¹³C NMR (126 MHz, CDCl₃) δ 160.26, 157.89, 151.45, 151.31, 150.51, 150.27, 148.37, 147.03, 137.22, 136.23, 134.99, 128.55, 128.53, 124.19, 122.87, 121.01, 120.55, 106.91, 106.74, 44.00, 41.31, 40.72, 38.72, 32.72, 21.06, 20.96, 13.21, 13.11; MS (ESI) *m/z* 533.30 [M + H]⁺.

N-Boc-3-(6-(2,5-Dimethyl-1H-pyrrol-1-yl)-4-methylpyridin-2-yl)-2-(6-(2-(6-(2,5-dimethyl-1H-pyrrol-1-yl)-4-methylpyridin-2-yl)ethyl)-pyridin-2-yl)propan-1-amine (30c). To a portion of the crude product of **30b** (~0.27 mmol, 150 mg) in 10 mL of dichloromethane was added Boc₂O (109 mg, 0.5 mmol) and triethylamine (70 μL, 0.5 mmol), and it was stirred for 12 h. The reaction mixture was concentrated in vacuo and then purified by flash chromatography (EtOAc/hexanes) to give the title compound (110 mg, 62%) as a colorless oil. The chiral resolution of racemic **30c** was performed using an OD-H chiral column with an autocollector-equipped HPLC system; **30c** (100 mg) was dissolved in 2 mL of EtOH, and then 0.1 mL of the solution per time was injected until the parent solution was all consumed. The separated enantiomers were collected and concentrated in vacuo to give **30c-1** (43 mg, *R*ₜ = 16.1 min, *ee* = 98%) and **30c-2** (32 mg, *R*ₜ = 23.1 min, *ee* = 97%). ¹H NMR (500 MHz, CDCl₃) δ 8.27 (s, 1H), 8.22 (s, 1H), 7.42 (s, 1H), 6.93 (s, 1H), 6.90 (s, 1H), 6.84 (s, 2H), 5.91 (s, 2H), 5.89 (s, 2H), 4.64 (d, *J* = 6.7 Hz, 1H), 3.55−3.37 (m, 3H), 3.35−3.24 (m, 1H), 3.24−3.14 (m, 1H), 3.06−2.93 (m, 3H), 2.39 (s, 3H), 2.33 (s, 3H), 2.15 (s, 6H), 2.07 (s, 6H), 1.40 (s, 9H); ¹³C NMR (126 MHz, CDCl₃) δ 160.02, 158.72, 155.74, 151.75, 151.64, 149.74, 149.69, 148.28, 147.32, 137.04, 136.73, 135.32, 128.42, 123.41, 122.64, 120.54, 120.33, 106.79, 106.67, 79.38, 45.18, 43.46, 41.36, 39.13, 32.69, 28.35, 21.02, 20.98, 13.30, 13.21; MS (ESI) *m/z* 654.56 [M + Na]⁺.

Computational Methods. The MM-PBSA method, as implemented in Amber 9.0[28] used in our previous work, was used to calculate free energies of binding. In this method, the total free energy of the NOS−inhibitor complex is taken as the sum of the following energy terms:

$$G = E_{MM} + G_{solv} + G_{np} - TS_{solute}$$

where E_{MM} = the total molecular mechanics energy computed with the Sander module in Amber 9.0, G_{solv} is the solvation free energy estimated from the Poisson−Boltzmann equation, G_{np} = the nonpolar solvation energy estimated from the solvent accessible surface area, and TS_{solute} = the solute entropy. From a single energy-minimized structure, the free energy is computed for the NOS−inhibitor complex, NOS alone with the inhibitor removed, and the inhibitor alone. The overall free energy of binding is computed from the following equation:

$$\Delta G_{bind} = (G_{complex} - G_{receptor} - G_{inhibitor})$$

As others have done, the solute entropy is ignored.[29] Given that the inhibitors used for these calculations are exactly the same, ignoring entropy introduces little error. Parameters for the inhibitor and heme were the same as described previously.[24]

Enzyme Assay Methods. All of the NOS isoforms were overexpressed and purified,[30−32] and enzyme kinetics data were determined using the hemoglobin capture assay (HCA) at 37 °C in a high-throughput method using 96-well plates. A typical assay mixture for nNOS and eNOS contained various concentrations of the test compound, 10 μM L-Arg, 1.0 mM CaCl₂, 300 units/mL calmodulin

(Sigma, P-2277), 100 μM NADPH, 0.125 mg/mL hemoglobin-A^0 (ferrous form, Sigma, H0267), and 10 μM H_4B in 100 mM HEPES (pH 7.5). A typical assay mixture for iNOS contained various concentrations of the test compound, 100 μM NADPH, 0.125 mg/mL hemoglobin-A^0 (ferrous form), and 10 μM H_4B in 100 mM HEPES (pH 7.5). All assays were in a final volume of 100 μL and were initiated by the addition of enzyme (approximately 100 nM final concentration). Nitric oxide-mediated oxidation of hemoglobin-A^0 was monitored at 401 nm for 1 min on a Synergy H1 reader by Biotek. Curves were fitted using the Michaelis–Menten equation in GraphPad Prism 5.0 (GraphPad Software, Inc.). For K_i determinations, IC_{50} values were calculated using nonlinear regressions (dose–response inhibition, four-parameter variable slope). Subsequent K_i values were calculated using the Cheng-Prusoff relationship: $K_i = IC_{50}/(1 + [S]/K_m)$ (K_m values used for rat nNOS, murine iNOS, bovine eNOS, and human nNOS were 1.3, 8.3, 1.7, and 1.6 μM respectively).

ASSOCIATED CONTENT

S **Supporting Information**

Synthesis of **28**, inhibitor complex crystal preparation, X-ray crystallographic data collection and refinement statistics, and ^{1}H and ^{13}C spectra of **3**, **4**, **5**, **6**, **7**, and **8**. This material is available free of charge via the Internet at http://pubs.acs.org.

AUTHOR INFORMATION

Corresponding Authors

*(T.L.P.) Phone: 949-824-7020. Fax: 949-824-3280. E-mail: poulos@uci.edu.

*(R.B.S.) Phone: 847-491-5653. Fax: 847-491-7713. E-mail: Agman@chem.northwestern.edu.

Notes

The authors declare no competing financial interest.

ACKNOWLEDGMENTS

ABBREVIATIONS USED

nNOS, neuronal nitric oxide synthase; iNOS, inducible nitric oxide synthase; eNOS, endothelial nitric oxide synthase; ALS, amyotrophic lateral sclerosis; FMN, flavin mononucleotide; MM-PBSA, molecular mechanics–Poisson–Boltzmann surface area

REFERENCES

(1) Ignarro, L. J. Nitric oxide as a unique signaling molecule in the vascular system: a historical overview. *J. Physiol. Pharmacol.* **2002**, *53* (4, Pt. 1), 503–514.

(2) Vallance, P.; Leiper, J. Blocking NO synthesis: how, where and why? *Nat. Rev. Drug Discovery* **2002**, *1*, 939–950.

(3) Alderton, W. K.; Cooper, C. E.; Knowles, R. G. Nitric oxide synthases: structure, function and inhibition. *Biochem. J.* **2001**, *357* (Pt 3), 593–615.

(4) Knowles, R. G.; Moncada, S. Nitric oxide synthases in mammals. *Biochem. J.* **1994**, *298*, 249–258.

(5) Li, H.; Forstermann, U. Nitric oxide in the pathogenesis of vascular disease. *J. Pathol.* **2000**, *190*, 244–254.

(6) Comini, L.; Boraso, A.; Bachetti, T.; Bernocchi, P.; Pasini, E.; Bastianon, D.; Curello, S.; Terracciano, C. M.; Ceconi, C.; Ferrari, R. Effects of endotoxic shock on neuronal NOS and calcium transients in rat cardiac myocytes. *Pharmacol. Res.* **2005**, *51*, 409–417.

(7) Smith, S. E.; Man, C. M.; Yip, P. K.; Tang, E.; Chapman, A. G.; Meldrum, B. S. Anticonvulsant effects of 7-nitroindazole in rodents with reflex epilepsy may result from L-arginine accumulation or a reduction in nitric oxide or L-citrulline formation. *Br. J. Pharmacol.* **1996**, *119*, 165–173.

(8) Ramachandran, R.; Ploug, K. B.; Hay-Schmidt, A.; Olesen, J.; Jansen-Olesen, I.; Gupta, S. Nitric oxide synthase (NOS) in the trigeminal vascular system and other brain structures related to pain in rats. *Neurosci. Lett.* **2010**, *484*, 192–196.

(9) Dorheim, M. A.; Tracey, W. R.; Pollock, J. S.; Grammas, P. Nitric oxide synthase activity is elevated in brain microvessels in Alzheimer's disease. *Biochem. Biophys. Res. Commun.* **1994**, *205*, 659–665.

(10) Giasson, B. I.; Duda, J. E.; Murray, I. V.; Chen, Q.; Souza, J. M.; Hurtig, H. I.; Ischiropoulos, H.; Trojanowski, J. Q.; Lee, V. M. Oxidative damage linked to neurodegeneration by selective alpha-synuclein nitration in synucleinopathy lesions. *Science* **2000**, *290*, 985–989.

(11) Norris, P. J.; Waldvogel, H. J.; Faull, R. L.; Love, D. R.; Emson, P. C. Decreased neuronal nitric oxide synthase messenger RNA and somatostatin messenger RNA in the striatum of Huntington's disease. *Neuroscience* **1996**, *72*, 1037–1047.

(12) Yang, Z.; Misner, B.; Ji, H.; Poulos, T. L.; Silverman, R. B.; Meyskens, F. L.; Yang, S. Targeting nitric oxide signaling with nNOS inhibitors as a novel strategy for the therapy and prevention of human melanoma. *Antioxid. Redox Signaling* **2013**, *19*, 433–447.

(13) Lian, K.; Murad, F. Nitric oxide (NO)-biogeneration, regulation, and relevance to human disease. *Front. Biosci.* **2003**, *8*, d264–d278.

(14) Holden, J. K.; Li, H.; Jing, Q.; Kang, S.; Richo, J.; Silverman, R. B.; Poulos, T. L. Structural and biological studies on bacterial nitric oxide synthase inhibitors. *Proc. Natl. Acad. Sci. U.S.A.* **2013**, *110*, 18127–18131.

(15) van Sorge, N. M.; Beasley, F. C.; Gusarov, I.; Gonzalez, D. J.; von Köckritz-Blickwede, M.; Anik, S.; Borkowski, A. W.; Dorrestein, P. C.; Nudler, E.; Nizet, V. Methicillin-resistant *Staphylococcus aureus* bacterial nitric-oxide synthase affects antibiotic sensitivity and skin abscess development. *J. Biol. Chem.* **2013**, *288*, 6417–6426.

(16) Mukherjee, P.; Cinelli, M. A.; Kang, S.; Silverman, R. B. Development of nitric oxide synthase inhibitors for neurodegeneration and neuropathic pain. *Chem. Soc. Rev.* **2014**, DOI: 10.1039/C3CS60467E.

(17) Ghosh, D. K.; Stuehr, D. J. Macrophage NO synthase: characterization of isolated oxygenase and reductase domains reveals a head-to-head subunit interaction. *Biochemistry* **1995**, *34*, 801–807.

(18) Raman, C. S.; Li, H.; Martásek, P.; Král, V.; Masters, B. S.; Poulos, T. L. Crystal structure of constitutive endothelial nitric oxide synthase: a paradigm for pterin function involving a novel metal center. *Cell* **1998**, *95*, 939–950.

(19) Woodward, J. J.; Nejatyjahromy, Y.; Britt, R. D.; Marletta, M. A. Pterin-centered radical as a mechanistic probe of the second step of nitric oxide synthase. *J. Am. Chem. Soc.* **2010**, *132*, 5105–5113.

(20) Li, H.; Poulos, T. L. Structure-function studies on nitric oxide synthases. *J. Inorg. Biochem.* **2005**, *99*, 293–305.

(21) Panda, K.; Rosenfeld, R. J.; Ghosh, S.; Meade, A. L.; Getzoff, E. D.; Stuehr, D. J. Distinct dimer interaction and regulation in nitric-oxide synthase types I, II, and III. *J. Biol. Chem.* **2002**, *277*, 31020–31030.

(22) Ji, H.; Delker, S. L.; Li, H.; Martásek, P.; Roman, L. J.; Poulos, T. L.; Silverman, R. B. Exploration of the active site of neuronal nitric oxide synthase by the design and synthesis of pyrrolidinomethyl 2-aminopyridine derivatives. *J. Med. Chem.* **2010**, *53*, 7804–7824.

(23) Xue, F.; Fang, J.; Delker, S. L.; Li, H.; Martásek, P.; Roman, L. J.; Poulos, T. L.; Silverman, R. B. Symmetric double-headed amino-pyridines, a novel strategy for potent and membrane-permeable inhibitors of neuronal nitric oxide synthase. *J. Med. Chem.* **2011**, *54*, 2039–2048.

(24) Delker, S. L.; Ji, H.; Li, H.; Jamal, J.; Fang, J.; Xue, F.; Silverman, R. B.; Poulos, T. L. Unexpected binding modes of nitric oxide synthase inhibitors effective in the prevention of a cerebral palsy phenotype in an animal model. *J. Am. Chem. Soc.* **2010**, *132*, 5437−5442.

(25) Fang, J.; Ji, H.; Lawton, G. R.; Xue, F.; Roman, L. J.; Silverman, R. B. L337H Mutant of rat neuronal nitric oxide synthase resembles human neuronal nitric oxide synthase toward inhibitors. *J. Med. Chem.* **2009**, *52*, 4533−4537.

(26) Flinspach, M. L.; Li, H.; Jamal, J.; Yang, W.; Huang, H.; Hah, J. M.; Gómez-Vidal, J. A.; Litzinger, E. A.; Silverman, R. B.; Poulos, T. L. Structural basis for dipeptide amide isoform-selective inhibition of neuronal nitric oxide synthase. *Nat. Struct. Mol. Biol.* **2004**, *11*, 54−59.

(27) Walia, A.; Kang, S.; Silverman, R. B. Microwave-assisted protection of primary amines as 2,5-dimethylpyrroles and their orthogonal deprotection. *J. Org. Chem.* **2013**, *78*, 10931−10937.

(28) Massova, I.; Kollman, P. A. Computational alanine scanning to probe protein-protein interactions: A novel approach to evaluate binding free energies. *J. Am. Chem. Soc.* **1999**, *121*, 8133−8143.

(29) Brown, S. P.; Muchmore, S. W. High-throughput calculation of protein-ligand binding affinities: modification and adaptation of the MM-PBSA protocol to enterprise grid computing. *J. Chem. Inf. Model.* **2006**, *46*, 999−1005.

(30) Hevel, J. M.; White, K. A.; Marletta, M. A. Purification of the inducible murine macrophage nitric oxide synthase: Identification as a falvoprotein. *J. Biol. Chem.* **1991**, *266*, 22789−22791.

(31) Gerber, N. C.; Ortiz de Montellano, P. R. Neuronal nitric oxide synthase. *J. Biol. Chem.* **1995**, *270*, 17791−17796.

(32) Martásek, P.; Liu, Q.; Liu, J.; Roman, L. J.; Gross, S. S.; Sessa, W. C.; Masters, B. S. S. Characterization of bovine endothelial nitric oxide synthase expressed in *E. coli. Biochem. Biophys. Res. Commun.* **1996**, *219*, 359−365.